NASA TECHNICAL REPORT

NASA TR R-299

NASA TR R-299

SOLUTIONS OF BLUNT-BODY STAGNATION-REGION FLOWS WITH NONGRAY EMISSION AND ABSORPTION OF RADIATION BY A TIME-ASYMPTOTIC TECHNIQUE

by Linwood B. Callis

Langley Research Center
Langley Station, Hampton, Va.

NATIONAL AERONAUTICS AND SPACE ADMINISTRATION • WASHINGTON, D. C. • JANUARY 1969

NASA TR R-299

SOLUTIONS OF BLUNT-BODY STAGNATION-REGION FLOWS WITH NONGRAY EMISSION AND ABSORPTION OF RADIATION BY A TIME-ASYMPTOTIC TECHNIQUE

By Linwood B. Callis

Langley Research Center
Langley Station, Hampton, Va.

NATIONAL AERONAUTICS AND SPACE ADMINISTRATION

For sale by the Clearinghouse for Federal Scientific and Technical Information
Springfield, Virginia 22151 – CFSTI price $3.00

SOLUTIONS OF BLUNT-BODY STAGNATION-REGION FLOWS WITH NONGRAY EMISSION AND ABSORPTION OF RADIATION BY A TIME-ASYMPTOTIC TECHNIQUE

By Linwood B. Callis
Langley Research Center

SUMMARY

A second-order time-asymptotic solution to radiation-coupled stagnation-region flows is presented. The solution is applied to the hypervelocity flow over blunt vehicles of inviscid, nonconducting, equilibrium air, emitting and absorbing nongray radiation. Velocities, nose radii, and altitudes covered by the analysis are sufficient to bracket reentry trajectories of current interest. Radiative heat-transfer rates for the range of interest and typical profiles of pressure, density, enthalpy, temperature, and velocity are shown. The nature of the time-asymptotic solution is discussed and it is shown to be a feasible means of achieving second-order accurate solutions to radiation-coupled shock-layer flows.

Step-function models of the absorption coefficient are used in order to evaluate the divergence of the radiation flux vector. An analysis is carried out to determine what effect variations in the spectral complexity of the step model absorption coefficients used in the analysis will have on the thermodynamic and flow profiles of interest and on the nongray radiative heat-transfer rates. In this connection use is made of consistent model absorption coefficients having one to nine spectral steps with free-free, free-bound (including atomic line transitions), and molecular transitions taken into account. Relatively simple models of the absorption coefficient can be used with no significant loss of accuracy. An existing correlation for the cooling factor, the ratio of the radiation heat-transfer rate to the adiabatic radiation heat-transfer rate, is extended to larger velocities than heretofore considered.

INTRODUCTION

During the past decade, problems involving radiation-coupled flow fields have received the attention of numerous investigators. It has been amply demonstrated (refs. 1 to 4) that the inclusion of the emission and absorption of radiation in stagnation flow-field analyses may significantly alter both the flow-field structure and the heat-transfer rates typically expected from radiationless solutions. For blunted vehicles entering the earth's

atmosphere, these effects manifest themselves at velocities in excess of 9 km/sec; this makes necessary the consideration of the coupling existing between the radiation transport equations and the fluid-dynamic equations governing the flow. The problem posed by such a consideration is extremely difficult since the solution is governed by a set of nonlinear, partial, integro-differential equations. Furthermore, the integral terms involve complicated functions of wavelength and spatial coordinates; therefore, tedious numerical integration is necessary.

The most general approaches to the problem to date are typified by the solutions of Howe and Viegas (ref. 1), Hoshizaki and Wilson (ref. 2), and Olstad (ref. 3). The solutions in references 1 and 2 are similar in that both consider the flow field to be totally viscous and conducting and both consider injection of foreign species as well as energy transport by diffusion. Howe and Viegas (ref. 1), assuming similarity, reduce their governing equations to a set of ordinary differential equations which are solved by standard techniques. The absorption coefficient is considered to be gray. Hoshizaki and Wilson (ref. 2) maintain variations in the body tangent direction. The energy equation is solved by finite-difference techniques with the velocity and species concentration profiles determined from an integral solution to the species continuity equation and the momentum equation. The analysis is for a nongray gas. Olstad (ref. 3) uses a Poincaré-Lighthill-Kuo singular perturbation technique to obtain stagnation region solutions for an inviscid, nonconducting gas with a nongray absorption coefficient. This solution involves expansions in terms of the radiation cooling parameter $4\delta_a\epsilon$ and is valid for $4\delta_a\epsilon \ll 1$.

The purpose of the present analysis is threefold. The first is to point out that time-asymptotic techniques are a practical means of solving nonadiabatic radiation-coupled flow fields. The techniques discussed herein have been used to generate radiation-coupled stagnation-line solutions, including emission and absorption of nongray radiation, and hopefully they will be applicable to the analysis of the full flow field. This particular approach was adopted as it seemed to offer a direct solution to the problem at hand with a minimum number of restrictive assumptions and computational difficulties. This advantage results in large part from the hyperbolic nature of the governing set of partial differential equations when cast in their unsteady form. Moretti and Abbett (ref. 5) have demonstrated that radiationless calculations can be carried on in the entire flow field with few of the usually attendant problems of convergence, stability, or sensitivity to initial guesses. The time-asymptotic approach used herein is essentially a second-order accurate Taylor series expansion in time of the quantities of interest. The solution is advanced in time until an asymptotic situation is reached representing the steady-state result.

Shock waves, with the aid of unsteady characteristics, are treated as discontinuities providing more accurate profiles in the vicinity of the shock front. In addition, use of a

discontinuous shock allows a coarser mesh to be used than is possible with the "artificial viscosity" technique (refs. 6 and 7); thereby, there is a considerable saving in computing time and storage. The second-order solutions presented in this report have been achieved in remarkably short computing times, typically 20 seconds/case or less on a Control Data series 6000 computer system. The present stagnation solution is thus offered as a demonstration of the feasibility of the time-asymptotic approach to the solution of general radiation-coupled flow fields as well as a valid solution in its own right.

The second purpose of the analysis is to determine what effect variations in the spectral complexity of the absorption coefficients used in the analysis will have on the thermodynamic and flow profiles of interest and on the nongray radiative heat-transfer rates. In this connection, use is made of data tabulated by Olstad (ref. 8) in formulating step models of the absorption coefficient with one to nine spectral steps. The radiative processes taken into account in the formulation of these step models are line transitions, N^+- and O^+-electron recombination, free-free electron interactions, and molecular-band system radiation. Solutions determined with model absorption coefficients constructed from the same detailed spectral information are compared and discussed.

Finally, radiation heat-transfer rates to a sphere are presented for velocities from 9 to 18 kilometers/second, nose radii from 0.1 to 10 meters, and altitudes from 49 to 73 kilometers. A comparison is made with the cooling factor correlation presented in reference 8, and the range of this correlation is extended.

SYMBOLS

A parameter defined by equations (A18) and (A23)

B, C, D, E, P_1, P_3 parameters defined by equations (A18)

B_ν nondimensional blackbody function

C_1, C_2, C_3 parameter defined by equations (B4), (B5), and (B6), respectively

E_n exponential integral function of order n, $E_n(Y) = \int_1^\infty e^{-Yt} t^{-n} dt$

F_R nondimensional divergence of the radiation flux vector

F_c cooling factor, $\frac{q_{R,w}}{q_{R,w,a}}$

f parameter defined by equation (A24)

g	parameter representing p, ρ, v, or f
h	nondimensional enthalpy
I_ν	nondimensional specific radiation intensity
K	parameter defined by equation (A10)
$\bar{k}$	Boltzmann constant, joules/^{o}K
p	nondimensional pressure
q_R	nondimensional radiation heat flux
r	radius defined by equation (A5)
$\overline{R}_N$	nose radius, meters
s	nondimensional incremental radiation path
T,t,t'	nondimensional time except where indicated
T*	parameter defined by equation (C6)
$\vec{U}$	nondimensional velocity vector
u,v	nondimensional velocity components
$\overline{V}_\infty$	free-stream velocity, meters/second
x',y',z'	nondimensional Cartesian coordinates
x,y	nondimensional body-oriented coordinates
X,Y	nondimensional floating coordinates
$\overline{Z}$	altitude, kilometers
α_1,α_2,β	parameters describing picket-fence model

β	angle between shock and body except where indicated, radians
δ	nondimensional standoff distance
ΔT	nondimensional time increment
ϵ	parameter defined by equation (A3)
η_i	parameter defined by equation (C7)
θ	body surface inclination, radians
$\overline{\lambda}$	wavelength, angstroms except where indicated
ν	nondimensional radiation frequency
$\overline{\rho}$	density, kilograms/meter^3
$\overline{\rho k}$	absorption coefficient, meter^{-1}
$\overline{\rho k}_p$	Planck mean absorption coefficient, meter^{-1}
$\overline{\sigma}$	Stefan-Boltzmann constant, watts/(meter-$^oK^4$)
τ	optical thickness
ϕ	azimuthal angle, radians
ω	solid angle, steradians

Subscripts:

a	adiabatic wall
o	standard atmospheric conditions
w	wall conditions
Δ	stationary shock conditions on center line

δ local unsteady shock conditions at time T

ν quantity evaluated at frequency ν

∞ free-stream conditions

Symbols with bars represent dimensional quantities, those without bars indicate nondimensional quantities.

ANALYSIS

Nondimensionalization

The equations appearing in this report are nondimensional. All distances are nondimensionalized by the vehicle nose radius $\overline{R}_N$, all time quantities by the ratio $\overline{R}_N/\overline{V}_\infty$, densities by $\overline{\rho}_\infty$, pressures by $\overline{\rho}_\infty \overline{V}_\infty^2$, energy flux by $\frac{1}{2}\overline{\rho}_\infty \overline{V}_\infty^3$, enthalpies by $\overline{V}_\infty^2$, the divergence of the radiation flux vector by $\overline{\sigma}\left(\overline{\rho k_p}\right)_\Delta \overline{T}_\Delta^4$ where $\overline{T}_\Delta$ is a temperature, velocities by $\overline{V}_\infty$, and absorption coefficients by $\left(\overline{\rho k_p}\right)_\Delta$.

Basic Assumptions and Flow Model

The basic assumptions under which the analysis is simplified and carried out are that

(1) The flow is axisymmetric, inviscid, and nonconducting

(2) The flow is in chemical equilibrium

(3) The shock wave and free stream are transparent to shock-layer radiation

(4) The body surface with regard to radiation is cold, nonreflecting, and black

(5) The tangent slab approximation is applicable

Basically these assumptions are made so that the applicability of the time-dependent techniques to radiation-coupled flows can be clearly determined free of other complicating phenomena. They are discussed at various points in the analysis. Figure 1 presents a schematic illustration of the flow geometry in the stagnation region of spherically blunted vehicle.

Procedure

The time-asymptotic approach in this report uses the following second-order accurate Taylor series expansion to advance an assumed solution in time until it becomes asymptotic to the desired steady-state solution:

$$g(Y,T+\Delta T) = g(Y,T) + g_T(Y,T)\Delta T + \frac{1}{2} g_{TT}(Y,T)\Delta T^2 + O(\Delta T^3) \tag{1}$$

The expansion furnishes a new value of the parameter g, which may represent p, ρ, v, or f, at the coordinates Y and $T + \Delta T$. This procedure is carried out at each Y coordinate of interest until all the information required for the continuation of the solution in time is available at $T + \Delta T$. Information on the shock and the body at $T + \Delta T$ is generated with the aid of the method of unsteady characteristics, discussed in the next section. Once the information at the next time plane is completely determined, the process is repeated until the variation between solutions at successive time planes is sufficiently small. This is taken as the steady-state result.

The first-order time derivatives are determined from the unsteady conservation equations developed in appendix A (eqs. (A20), (A21), (A22), (A23), and (A25)). These equations are given here as follows:

$$\rho_T = -\left(A\rho_Y + \frac{2\rho f}{\lambda} + \frac{\rho v_Y}{\delta} + \frac{2K\rho v}{\lambda}\right)$$

$$v_T = -\left(Av_Y + \frac{1}{\rho\delta} p_Y\right)$$

$$p_T = -\left[Ap_Y + P_3\left(\frac{2\rho f}{\lambda} + \frac{\rho v_Y}{\delta} + \frac{2\rho vK}{\lambda}\right) - \frac{\epsilon F_R}{P_1\rho}\right]$$

$$A = \frac{v}{\delta} - \frac{Y\delta_T}{\delta}$$

$$f_T = -\left(Af_Y + \frac{f^2}{\lambda} + \frac{Kfv}{\lambda} + \frac{p_{XX}}{\rho\lambda}\right)$$

The right-hand side of equations (A20), (A21), (A22), (A23), and (A25) (hereafter referred to as set 1) are evaluated by using data on the most recent time plane. All derivatives, with the exception of p_{XX}, are determined by centered finite difference representation. At this point, it is necessary to determine values for p_{XX}. This is accomplished by assuming that at the center line the shock wave is concentric with the body so that

$$p_{XX} = -2\left(1 - \frac{1}{\rho_\delta}\right) \tag{2}$$

Equation (2), derived from steady-flow shock relations, is admittedly inconsistent with the unsteady nature of the analysis. The consequences of this inconsistency are not serious, however, since the momentum equation is only weakly coupled to the energy equation and since a steady-state solution is ultimately sought. Hence, use of equation (2)

involves some error in the intermediate development of the solution but little in the final results.

Second-order time derivatives in equation (1) are obtained by differentiating set 1 with respect to T. The mixed space-time derivatives that result are evaluated by differentiating set 1 with respect to Y and using centered finite differences where applicable. Time derivatives of quantities such as P_3, P_1, F_R, and A are cast as backward time differences by using the most recent time data and data from the previous time plane. The result of these manipulations is a set of equations for the required first and second time derivatives of p, ρ, f, and v. These derivatives used in equation (1) permit the solution to advance in time.

Analysis of Shock and Body Points

A quasi-one-dimensional unsteady characteristics technique, similar to that used by Moretti and Abbett (ref. 5) was applied to the analysis of the shock wave in order to retain the shock as a discrete surface. Artificial viscosity techniques have the effect of smearing the shock until it becomes not a discrete surface but a region having large flow property gradients. The distinction between the two approaches can, for radiation-coupled flows, be an important one since the enthalpy level can be significantly reduced in a region near the shock front. Consequently, poor shock definition can result in a poorly defined enthalpy profile. A schematic of the flow field (fig. 2) near the shock serves to illustrate how the characteristics method is applied. The shock standoff distance δ varies with T. At time T all quantities are known across the shock layer and it is desired to know $\delta(T + \Delta T)$, $\delta_T(T + \Delta T)$, and values of the flow properties at point A. As an initial guess, it is assumed that $\delta_T(T + \Delta T) = \delta_T(T)$ and that $\delta(T + \Delta T) = \delta(T) + \delta_T(T)\Delta T$; thus, point A is located and, with the aid of the Rankine-Hugoniot relations, conditions are determined at A in the shock layer. A right running characteristic (see appendix B), indicated in figure 2, is extended in the negative time direction until B is located. The location of B is stabilized by an iterative process averaging the slope of the right running characteristic between A and B. Once point B is stabilized, the compatibility relation (eq. (B11)) is integrated from point B to point A with averaged coefficients and a value of v at point A determined. If the computed v does not match the value obtained from the Rankine-Hugoniot equations a new value of $\delta_T(T + \Delta T)$, consistent with v and A as determined from the compatibility equations, is calculated and the entire procedure cycled to convergence. This procedure yields conditions at point A and is carried out prior to the advancement of interior flow properties to $T + \Delta T$.

At the body, the procedure is similar. The slope of the left running characteristic (fig. 2) is assumed at A' and extended in negative time until point B' is located. Point B' is stabilized by iteration and the proper compatibility relation (eq. (B11)) integrated from

B' to A' to determine the pressure at A'. The unsteady energy equation is then integrated from C' to A' to determine the enthalpy at A'. Values of h and p permit a new calculation of the characteristic slope at A' and the procedure is cycled to convergence.

Computation of the Divergence of the Radiation Flux Vector

The calculation of the divergence of the radiation flux vector F_R is carried out under the assumptions and by the means indicated in appendix C. It has been determined that F_R need not be calculated for each time cycle but may be evaluated, held fixed for several cycles, and then recomputed. This saves considerable computational time and has a negligible influence on the final result. The transient portion of the solution obviously will differ from that in which F_R is determined anew each cycle.

Step Model Absorption Coefficient

The difficulty of and the time consumed in the calculation of the divergence of the radiation flux vector F_R is strongly dependent on the spectral complexity of the absorption coefficient used. If a true replica of the absorption coefficient including line, free-bound, and free-free transitions were used, the computation time for F_R would be such that general flow-field calculations about blunted bodies would be impractical. As a result, various simplifications to the detailed absorption coefficient have been offered. The most obvious approximation and, also, the crudest is the gray approximation in which the absorption coefficient is allowed to vary with temperature and density but not with wavelength. The gray coefficient is usually the Planck mean of the true absorption coefficient. This approximation is unacceptable since it eliminates spectral detail which may be important when the shock layer is not optically thin in all spectral regions. A second approximate way to represent the absorption coefficient is to use two or more spectral steps to model the true coefficient.

The height or value of ρk for each of the steps varies with temperature and density but not with wavelength over the spectral extent of the step. Clearly, with the addition of a large number of steps, the coefficient may be approximated as closely as desired.

The approach adopted herein is that, for engineering purposes, an adequate representation of the absorption coefficient can be realized with a step model. The two-step, three-step, and nine-step models of ρk used in this report are discussed in appendix D and summarized in tables I and II. For comparison purposes a gray model is included. A schematic of these models is shown in figure 3.

Equilibrium Air Properties

Expressions used in this report relating pressure and sound speed to ρ and h for equilibrium air are presented by Cohen (refs. 9 and 10) or have been derived from data presented in these references. For the temperature, correlations due to Olstad have been used. More exact thermodynamic data, either tabulated or calculated, were not used in an effort to save computational time and in the interest of program simplicity. With regard to the general accuracy of the overall solution, it is felt that uncertainties in the absorption coefficient information generally available outweigh the slight errors due to the use of thermodynamic correlations.

Stability

The stability requirement applied to the present analysis is the CFL (Courant-Friedricks-Lewy) criterion used by Moretti and Abbett (ref. 5). The point of view was adopted that no consideration (other than optimization of the time increment) would be given to stability analyses unless instabilities developed in the solution. Since no such instabilities were encountered during the development and utilization of the present solution, the inclusion of a stability analysis is omitted. The application of the CFL criterion has proved satisfactory.

The uniqueness of the present solutions was determined by the execution of a number of different cases with significantly different initial conditions. In each case, variations of the initial conditions caused the final result to be changed by less than 1/2 percent. This observation and comparisons with other solutions led to the conclusion that no uniqueness problems existed.

RESULTS AND DISCUSSION

The analysis described has been successfully applied to flow situations with $9 \leq \overline{V}_\infty \leq 20$ km/sec, $0.01 \leq \overline{R}_N \leq 10$ m, $36 \leq \overline{Z} \leq 73$ km. Typical results for p, ρ, v, T, and h are shown in figure 4. The variations in ρ and h are as expected for a radiation-coupled flow field. Figure 5 depicts the variation in the enthalpy profile for three values of $\overline{V}_\infty$. The enthalpy level is reduced as $\overline{V}_\infty$ increases because of the increased energy lost by radiation from the shock layer. A similar variation in the enthalpy level is apparent as the nose radius $\overline{R}_N$ is increased. (See fig. 6.) Variation of the nondimensional standoff distance with both $\overline{R}_N$ and $\overline{V}_\infty$ is shown in figure 7. At the smaller values of $\overline{R}_N$, δ approaches its adiabatic value, whereas at larger values of $\overline{R}_N$, δ is significantly reduced as a result of the higher density levels in the shock layer.

The results shown in figures 4 to 7 demonstrate that the present time-asymptotic technique can be used successfully in the analysis of radiation-coupled flows. Results presented in this report cover the widest range of conditions yet published for a single solution. Validation of these results is accomplished by comparison with the work of reference 8, which uses an absorption coefficient identical to that shown in table I, and by comparison with the work of several other authors using different absorption coefficients. These comparisons are included in the discussion of figures 10 and 11, respectively. Typical computing times for the solutions are approximately 20 seconds/case or less (Control Data series 6000 computer system) making the technique attractive from the standpoint of practical usage. Computing times are relatively independent of $\overline{V}_\infty$, $\overline{R}_N$, and $\overline{Z}$.

Figure 8 shows, for a typical velocity and ambient density and a range of nose radii, the contribution to the total radiative heat flux by the various spectral steps of the nine-step model. For this case, the equilibrium mole fractions of selected air species are given at the shock and body in table III $\left(\overline{R}_N = 1 \text{ m}\right)$. Several observations can be made from figure 8, the first being that the largest single contribution to the total flux for all $\overline{R}_N$ comes from step 9, which has the smallest optical thickness. For $\overline{R}_N \gtrapprox 1.5$ meters this contribution is larger than the sum of the remaining contributions, an indication of the effect of reabsorption on the contribution from the more optically thick steps. A second point of interest is the relatively modest contribution made by the line centers, steps 4, 6, and 8. Steps 4 and 6 contribute such a minor amount that they may be combined with other steps with very little error. Step 8, however, can be as much as 6 to 10 percent of the total at small $\overline{R}_N$. Its identity should be preserved. Steps 1, 2, 3, and 5 all contribute heavily at small $\overline{R}_N$. These steps, together with 4 and 6, are combined according to a Planck average to form a single step existing spectrally from 400 to 1130 Å. Two other steps may be formed by the combination of 7 and 9 which behave similarly and by the remaining step 8. The result is the three-step model indicated in table II. The two-step model of table II is formed with the inclusion of step 8 with steps 7 and 9.

It should be noted here that the values of the absorption coefficient for steps 4, 6, and 8 are based on Griem's f-numbers (ref. 11, the best available when the model was formulated) which, according to more recent information, may be low by an order of magnitude. If updated values of the f-numbers were used, conclusions concerning the effect of the line centers on the heat flux may be modified. However, the same type of argument could be applied.

Figures 9 and 10, for a typical flow condition, show the effect, on both the heat-transfer rate and the enthalpy profiles, of using the nine-step, three-step, two-step, and gray absorption coefficients. If the nine-step model is accepted as being most nearly representative of the exact absorption coefficient, it is clear that the gray model is

unacceptable except for qualitative analysis, the enthalpy profile being in error by as much as 30 percent. The three-step model has a maximum enthalpy error of approximately 3 percent and the two-step model of 15 percent. This is an indication that the contribution of the line centers, given by step 8, should be maintained as a separate step. A large nose radius (in this case, 8 meters) emphasizes the defects of the two- and three-step models. In figure 10, stagnation-point heating rates are compared with those of reference 8 over a range of $\overline{R}_N$ and two values of $\overline{V}_\infty$. It should be pointed out that the solutions of reference 8 use the nine-step absorption coefficient (table I), whereas the present solutions are for both the nine-step and the three-step models (table II). The solutions of Olstad (ref. 8) are terminated at values of $\overline{R}_N$ and $\overline{V}_\infty$ at which the approximations of the small perturbation solution begin to be suspect. It is felt that some of the divergence between the solutions at the larger nose radii can be attributed to the onset of the breakdown of the small perturbation solution. Over most of the range of $\overline{R}_N$, however, the agreement is excellent, slight differences in the level of the two nine-step models being attributed to the use of different thermodynamic correlations. The close agreement between solutions using the three- and nine-step models is interesting in light of the variation of the complexity of the step models used.

In figure 11, the present stagnation-point heating rates are compared (for a range of $\overline{V}_\infty$ and p_Δ/p_0) with those of Hoshizaki and Wilson (ref. 2), Wilson and Hoshizaki (ref. 12), Chin (ref. 13), and Page, Compton, Borucki, Cliffone, and Cooper (ref. 14). All these references, with the exception of reference 2, include the effects of line radiation. Figure 11, though not the best way to present a comparison of solutions, is convenient since most of the data included were readily available in this form. (See ref. 14.) As seen from figure 11, the data of Wilson and Hoshizaki (ref. 12) with $p_\Delta/p_0 = 0.3$ and 0.4 compare very well with the present data for $0.08 < p_\Delta/p_0 \leq 0.2$, the radiation heat-transfer rate being weakly proportional to p_Δ/p_0. The data of Chin and of Page and coworkers (refs. 13 and 14, respectively) appear to be slightly low over the velocity range shown. The data of Hoshizaki and Wilson (ref. 2) which take into account continuum radiation only are 41 percent below the present result emphasizing the importance of line transitions. In general, however, the comparisons shown in figure 11 are satisfactory.

Figure 12 presents, for a spherically tipped body, a range of stagnation-point radiation heat-transfer solutions calculated by using the three-step absorption-coefficient model. Solutions are given for a range of $\overline{R}_N$ and values of $\overline{V}_\infty$ and $\overline{Z}$ sufficient to bracket most reentry conditions of interest.

In reference 8, Olstad presents a correlation of the cooling factor F_c, the ratio of the stagnation-point radiation heat-transfer rate $q_{R,w}$ to the adiabatic radiant heat-transfer rate $q_{R,w,a}$, both heating rates including the effects of absorption. The cooling factor is correlated as a function of $q_{R,w,a}$ for various altitudes and nose radii and for a fixed velocity.

Figure 13 presents these correlations for F_C as they appear in reference 8. The present solution has been used to extend the velocity range to 18 280 m/sec and to extend the correlations to larger values of $q_{R,w,a}$. For values of $q_{R,w,a}$ such that both solutions are equally applicable, excellent agreement is obtained. At the larger values of $q_{R,w,a}$, there is a tendency for the solutions to diverge, the present solutions having slightly higher values of F_C. This is attributed to the aforementioned onset of the breakdown of the small perturbation solution of reference 8. For further comparison, data from references 2 and 15 are indicated in figure 13(c), all falling well within the correlation limits. The data of Hoshizaki and Wilson (ref. 2) include no effect of line radiation, whereas the data of Rigdon, Dirling, and Thomas (ref. 15) use a modified hydrogenic approximation. In terms of absolute heating rates, agreement between the results of these references and the present results could differ by as much as 40 percent. (See fig. 11.) However, the good agreement of the data of references 2, 8, and 15 and the present data when correlated as in figure 13 is taken as a substantial indication of the validity of the correlation and its effectiveness in taking out the effect of variations in the absorption coefficient.

In light of these observations, it appears reasonable for an investigator to devote considerable effort to an accurate determination of $q_{R,w,a}$ (essentially a constant temperature calculation) with the best available absorption coefficient. The quantity $q_{R,w,a}$ may be translated with a high degree of accuracy (5 percent) to the desired heating rate $q_{R,w}$. This procedure would eliminate many of the difficulties and much of the time associated with the fully coupled calculation. The determination of $q_{R,w}$ could be further simplified by the compilation of tables of $q_{R,w,a}$ for a range of conditions. This would be useful for design purposes.

CONCLUDING REMARKS

It is felt that the present analysis successfully demonstrates the applicability of time-asymptotic techniques to the solution of inviscid, nonconducting flows including the effects of emission and absorption of nongray radiation. The advantages of the method are that it is accurate to second order, that few approximations are necessary, that little computational time is required, that solutions are insensitive to initial input, and that no stability problems are encountered if the CFL stability criterion is satisfied. With regard to full flow-field calculations, solutions are direct and may be easily extended through the sonic line with few of the usually attendant problems of other methods.

The effect of the variation of the spectral complexity of the model absorption coefficients on the final solution profiles and heat-transfer rates has been investigated. It has been found that the three-step model can be used to adequately represent the nine-step model over a range of velocities and nose radii. The question raised at this point

is whether or not a simplified model of the absorption coefficient (such as the nine-step model or one more sophisticated) can be used in practical calculations and yield sufficiently accurate results (less than 15-percent error) when compared with calculations using detailed spectral absorption coefficients. Obviously the only rigorous way to answer the question is to calculate both divergence of the radiation flux vector and the energy flux throughout a nonisothermal slab using detailed spectral information. These calculations should then be compared to similar calculations using modeled absorption coefficients derived from the detailed spectral information. To the author's knowledge, this has not yet been done. It is felt, however, that the present analysis strongly indicates that the detailed absorption can be simply modeled and these models used to achieve results with good accuracy and the retention of all significant trends. If full flow-field calculations are to be carried out, such work would be greatly facilitated by the use of modeled absorption coefficients.

A wide range of stagnation-point radiation heat-transfer solutions is presented which allows a direct determination of the heating rate for the nose radii, velocities, and altitudes shown. In addition, extensions of previously published cooling factor correlations have been made and are presented. These extensions allow the determination of the radiation heating rate for arbitrary altitudes, nose radii, and (within certain limits) absorption coefficients. Required for this determination is the velocity of the vehicle and a calculation of adiabatic wall heat flux by using the chosen absorption coefficient. Use of these correlations greatly simplifies the determination of the nongray radiation heat transfer for fully coupled flows and should prove valuable for design work.

Langley Research Center,
National Aeronautics and Space Administration,
Langley Station, Hampton, Va., September 24, 1968,
129-01-03-09-23.

APPENDIX A

COORDINATE SYSTEM AND BASIC EQUATIONS

Coordinate System

The coordinate system used in the analysis is a "floating" system (sketch A1) obtained from a transformation of body-oriented coordinates (t,x,y) for axisymmetric flow (sketch A2). The procedure will be to transform the equations of motion from the Cartesian system (t',x',y',z') to the body-oriented system, then to recast these relations in the "floating" coordinates (T,X,Y).

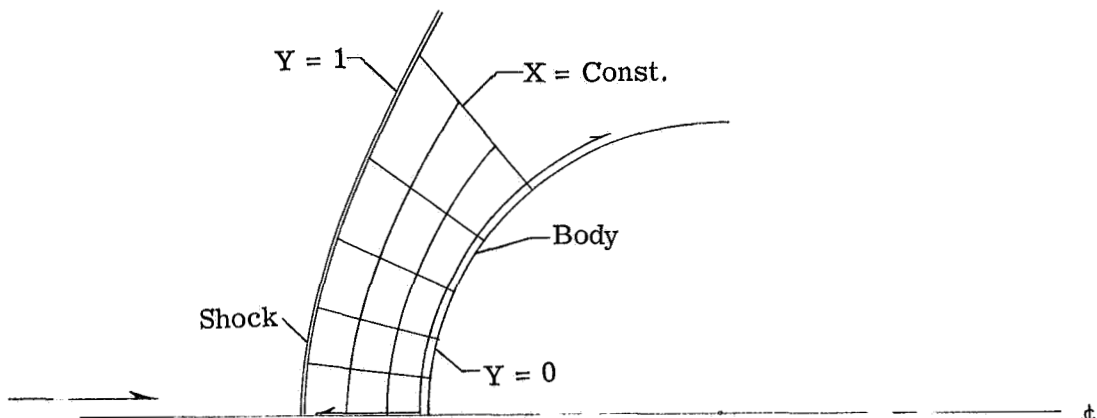

Sketch A1

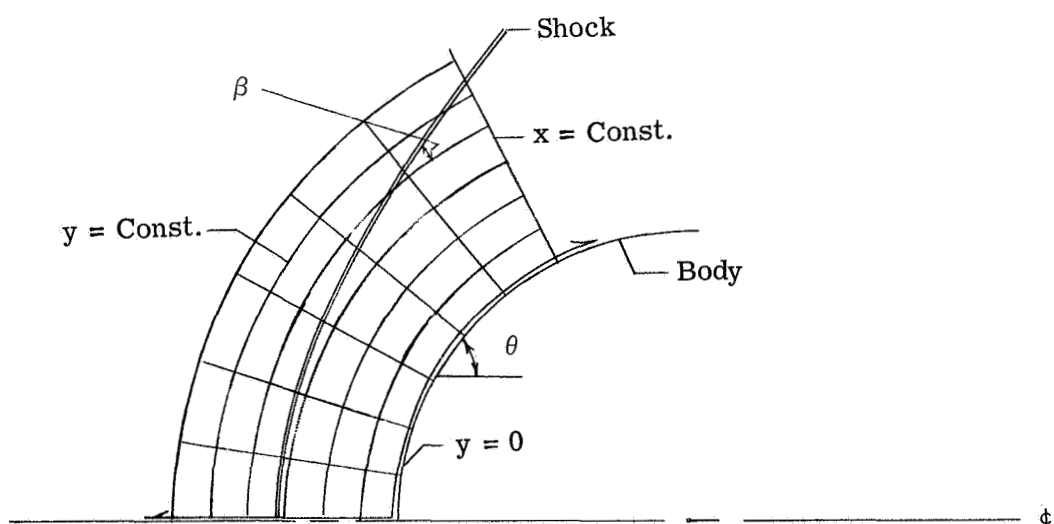

Sketch A2

APPENDIX A

Basic Equations

The following unsteady inviscid, nonconducting equations, including radiation effects, are given as follows:

Continuity

$$\frac{\partial \rho}{\partial t'} + \nabla \cdot \left(\rho \vec{U}\right) = 0 \tag{A1}$$

Momentum

$$\frac{\partial \vec{U}}{\partial t'} + \vec{U} \cdot \nabla \vec{U} = -\frac{1}{\rho} \nabla p \tag{A2}$$

Energy

$$\left.\begin{aligned} \frac{\partial h}{\partial t'} + \vec{U} \cdot \nabla h &= -\frac{\epsilon F_R}{\rho} + \frac{1}{\rho}\frac{\partial p}{\partial t'} + \frac{\vec{U} \cdot \nabla p}{\rho} \\ \epsilon &= \frac{\bar{\sigma} \bar{R}_N \left(\overline{\rho k_p}\right)_\Delta \bar{T}_\Delta^4}{\bar{\rho}_\infty \bar{V}_\infty^3} \end{aligned}\right\} \tag{A3}$$

The relations governing the transformation from the Cartesian coordinates (t',x',y',z') to the body-oriented system (t,x,y) are as follows:

$$\left.\begin{aligned} t' &= t \\ x' &= \int \cos\,\theta\, dx - y \sin\,\theta \\ y' &= r \sin\,\phi \\ z' &= r \cos\,\phi \end{aligned}\right\} \tag{A4}$$

where

$$r = \int \sin\,\theta\, dx + y \cos\,\theta \tag{A5}$$

If the proper transformation equations are applied and, for axisymmetric flow, the azimuthal components ignored, equations (A1) to (A3) become, in the body-oriented system,

Continuity

$$\frac{\partial \rho}{\partial t} + \frac{1}{\lambda}\frac{\partial}{\partial x}(\rho u) + \frac{\rho u}{r} \sin\,\theta + \frac{\partial}{\partial y}(\rho v) + \rho v\left(\frac{K}{\lambda} + \frac{\cos\,\theta}{r}\right) = 0 \tag{A6}$$

x-momentum

$$\frac{\partial u}{\partial t} + \frac{u}{\lambda}\frac{\partial u}{\partial x} + v\frac{\partial u}{\partial y} + \frac{Kuv}{\lambda} = -\frac{1}{\rho\lambda}\frac{\partial p}{\partial x} \tag{A7}$$

y-momentum

$$\frac{\partial v}{\partial t} + \frac{u}{\lambda}\frac{\partial v}{\partial x} + v\frac{\partial v}{\partial y} - \frac{Ku^2}{\lambda} = -\frac{1}{\rho}\frac{\partial p}{\partial y} \tag{A8}$$

Energy

$$\frac{\partial h}{\partial t} + \frac{u}{\lambda}\frac{\partial h}{\partial x} + v\frac{\partial h}{\partial y} = \frac{1}{\rho}\frac{\partial p}{\partial t} + \frac{u}{\rho\lambda}\frac{\partial p}{\partial x} + \frac{v}{\rho}\frac{\partial p}{\partial y} - \frac{\epsilon F_R}{\rho} \tag{A9}$$

where

$$\left.\begin{aligned} \lambda &= 1 + Ky \\ K &= -\frac{\partial \theta}{\partial x} \end{aligned}\right\} \tag{A10}$$

It would be convenient, if during the unsteady calculation the shock itself became a coordinate line as well as the body. This is accomplished through the transformation to the "floating" coordinate system shown as follows:

$$\left.\begin{aligned} T &= t \\ X &= x \\ Y &= \frac{y}{\delta} \end{aligned}\right\} \tag{A11}$$

which gives for $y = 0$, $Y = 0$ and for $y = \delta$, $Y = 1$. The differential relationships between the two coordinate systems are given below

$$\left.\begin{aligned} \frac{\partial(\ )}{\partial t} &= \frac{\partial(\ )}{\partial T} - \frac{Y}{\delta}\frac{\partial \delta}{\partial T}\frac{\partial(\ )}{\partial Y} \\ \frac{\partial(\ )}{\partial x} &= \frac{\partial(\ )}{\partial X} - \frac{Y}{\delta}\lambda_\delta \tan\beta \frac{\partial(\ )}{\partial Y} \\ \frac{\partial(\ )}{\partial y} &= \frac{1}{\delta}\frac{\partial(\ )}{\partial Y} \end{aligned}\right\} \tag{A12}$$

With the state equation,

$$h = h(p,\rho) \tag{A13}$$

and switching to p as the dependent variable in the energy equation, equations (A6) to (A10) under the transformation (A11) become

APPENDIX A

Continuity

$$\rho_T = -\left(A\rho_Y + \frac{u}{\lambda}\rho_X - Bu_Y + \frac{\rho}{\lambda}u_X + \frac{\rho}{\delta}v_Y + C\right) \tag{A14}$$

X-momentum

$$u_T = -\left(Au_Y + \frac{u}{\lambda}u_X - \frac{B}{\rho^2}p_Y + \frac{1}{\rho\lambda}p_X + D\right) \tag{A15}$$

Y-momentum

$$v_T = -\left(Av_Y + \frac{u}{\lambda}v_X + \frac{1}{\rho\delta}p_Y - E\right) \tag{A16}$$

Energy

$$p_T = -\left[Ap_Y + \frac{u}{\lambda}p_X + P_3\left(\frac{\rho}{\lambda}u_X - Bu_Y + \frac{\rho}{\delta}v_Y + C\right) - \frac{\epsilon F_R}{P_1\rho}\right] \tag{A17}$$

Subscript notation has been used to denote partial differentiation. The parameters in the equations are defined by the following relations:

$$\left.\begin{aligned}
A &= \frac{v}{\delta} - \frac{Y\delta_T}{\delta} - \frac{uY}{\delta}\tan\beta\,\frac{\lambda_\delta}{\lambda} \\
B &= \frac{\lambda_\delta}{\lambda}\frac{\rho Y}{\delta}\tan\beta \\
C &= \frac{\rho u}{r}\sin\theta + \rho v\left(\frac{K}{\lambda} + \frac{\cos\theta}{r}\right) \\
D &= \frac{Kuv}{\lambda} \\
E &= \frac{Ku^2}{\lambda} \\
P_3 &= \frac{\partial h/\partial\rho}{\frac{1}{\rho} - \frac{\partial h}{\partial p}} \\
P_1 &= \frac{1}{\rho} - \frac{\partial h}{\partial p}
\end{aligned}\right\} \tag{A18}$$

Equations (A14) to (A18) are valid for inviscid, nonconducting, equilibrium flows over smooth blunt bodies including emission and absorption of nongray radiation.

For this analysis these equations must be reduced so that they are applicable to stagnation-line flows. Symmetry dictates the following conditions at the stagnation line:

$$\left.\begin{aligned} u = u_Y &= 0 \\ \rho_X = v_X = h_X = p_X &= 0 \\ \beta &= 0 \\ \theta &= \frac{\pi}{2} \end{aligned}\right\} \tag{A19}$$

Indeterminant terms such as $\frac{\rho u \sin\theta}{r}$ and $\frac{\rho v \cos\theta}{r}$ are evaluated with the aid of L'Hospital's rule. Equations (A14) to (A18) now reduce to the following set:

Continuity

$$\rho_T = -\left(A\rho_Y + \frac{2\rho}{\lambda} u_X + \frac{\rho v_Y}{\delta} + \frac{2K\rho v}{\lambda}\right) \tag{A20}$$

Y-momentum

$$v_T = -\left(Av_Y + \frac{1}{\rho\delta} p_Y\right) \tag{A21}$$

Energy

$$p_T = -\left[Ap_Y + P_3\left(\frac{2\rho}{\lambda} u_X + \frac{\rho v_Y}{\delta} + \frac{2\rho vK}{\lambda}\right) - \frac{\epsilon F_R}{P_1\rho}\right] \tag{A22}$$

where under the stagnation line restrictions (eqs. (A19)),

$$A = \frac{v}{\delta} - \frac{Y\delta_T}{\delta} \tag{A23}$$

Equation (A15), the X-momentum equation, becomes degenerate at the stagnation line and seemingly offers no useful information. However, if equation (A7) is differentiated with respect to x, restricted to the stagnation line, and expressed in terms of the defined quantity f, where

$$f \equiv u_X = u_X \tag{A24}$$

the following differential equation for f is obtained:

$$f_T = -\left(Af_Y + \frac{f^2}{\lambda} + \frac{Kfv}{\lambda} + \frac{p_{XX}}{\rho\lambda}\right) \tag{A25}$$

after transformation to the (T,X,Y) system. This equation is necessary because of the appearance in equations (A20) and (A22) of u_X.

The governing differential equations are now (A20), (A21), (A22), and (A25).

APPENDIX B

DEVELOPMENT OF UNSTEADY CHARACTERISTICS EQUATIONS IN FLOATING COORDINATE SYSTEM

A quasi-one-dimensional unsteady characteristics solution, similar to that reported in reference 5, is used for the shock and body points. The compatibility equations and characteristic directions are determined from the general equations cast in the following form. The asterisks in equations (B1) and (B4) indicate that it is the natural logarithm of ρ that is differentiated.

$$\rho_T{}^* + A\rho_Y{}^* + \frac{1}{\delta} v_Y = C_1 \tag{B1}$$

$$v_T + Av_Y + \frac{1}{\rho\delta} p_Y = C_2 \tag{B2}$$

$$p_T + Ap_Y + \frac{P_3\rho}{\delta} v_Y = C_3 \tag{B3}$$

where

$$C_1 = -\left(\frac{u}{\lambda}\rho_X{}^* + \frac{f}{\lambda} - \frac{B}{\rho} u_Y + \frac{C}{\rho}\right) \tag{B4}$$

$$C_2 = -\left(\frac{u}{\lambda} v_X - E\right) \tag{B5}$$

$$C_3 = -\left[\frac{u}{\lambda} p_X + P_3\left(\frac{\rho}{\lambda} f + C\right) - \frac{\epsilon F_R}{P_1\rho} - P_3 B u_Y\right] \tag{B6}$$

At this point, it should be noted that, in the vicinity of the shock wave, the pertinent quantities are the normal component of the velocity and the Y-coordinate. The tangential velocity is unchanged across the shock and for smooth bodies the tangential derivatives of the flow properties are, for the most part, small in comparison with other terms. These observations coupled with the fact that for hypervelocity flows, the Y coordinate in the "floating" system is nearly normal to the shock (it is normal on the stagnation line for axisymmetric flow) suggest treating the terms represented by C_1, C_2, and C_3 as driving terms and employing a one-dimensional characteristics treatment of the shock point. The same basic argument can be made with regard to body points and it is for these reasons that equations (B1) to (B3) are cast in their present form. A variation of this basic technique was discussed by Moretti in reference 16 and more detailed information can be found in that publication.

To determine the characteristic directions for equations (B1) to (B3) and the following differential relations:

$$\frac{\partial \rho^*}{\partial T} dT + \frac{\partial \rho^*}{\partial Y} dY = d\rho^* \tag{B7}$$

$$\frac{\partial v}{\partial T} dT + \frac{\partial v}{\partial Y} dY = dv \tag{B8}$$

$$\frac{\partial p}{\partial T} dT + \frac{\partial p}{\partial Y} dY = dp \tag{B9}$$

the associated coefficient determinant is set equal to zero and expanded. The resulting cubic in dY/dT is solved and the characteristic directions are found to be

$$\frac{dY}{dT} = \begin{cases} A \\ A \pm \sqrt{P_3/\delta^2} \end{cases} \tag{B10}$$

The compatibility equations are determined by replacing a column of the coefficient determinant by the column formed by the right-hand side of equations (B1) to (B3) and (B7) to (B9). Expanding the resulting determinant and substituting equation (B10) yields the following equation:

$$\frac{dv}{dT} \pm \frac{1}{\rho\sqrt{P_3}} \frac{dp}{dT} = C_2 \pm \frac{C_3}{\rho\sqrt{P_3}} \tag{B11}$$

Equations (B1) to (B11) are valid for general flow fields. For axisymmetric stagnation-line flow equations (B10) and (B11) maintain the same general form; however, A is given by equation (A23) rather than equation (A18), $C_2 = 0$, and C_3 becomes

$$C_3 = -\left[\frac{2\rho P_3}{\lambda}(f + Kv) - \frac{\epsilon F_R}{P_1 \rho}\right] \tag{B12}$$

APPENDIX C

EVALUATION OF THE DIVERGENCE OF THE RADIATION FLUX VECTOR

It is desired to derive and determine a means of evaluating the expression for the divergence of the radiation flux vector at points across the shock layer. The shock layer at the stagnation line is modeled as an infinite gas slab of thickness δ with one boundary transparent to incident radiation and nonemitting. The other boundary, representing the body surface, is to be a cold, nonemitting, reflecting surface. Properties are assumed to vary only with the normal coordinate, and local thermodynamic equilibrium is assumed.

The nondimensional divergence of the flux vector is represented by the integral

$$F_R = \int_0^\infty \int_{4\pi} \frac{\partial I_\nu}{\partial s} \, d\omega \, d\nu \tag{C1}$$

where I_ν is the specific intensity of the radiation, and ds an incremental length along the path a pencil of radiation travels. The radiative transfer equation is substituted and after integrating there results

$$F_R = 4(\rho k_p)T^4 - \int_0^\infty \int_{4\pi} (\rho k_\nu) I_\nu \, d\omega \, d\nu \tag{C2}$$

If I_ν, as determined from a solution of the radiative transfer equation, is substituted and the proper boundary conditions applied, equation (C2) becomes

$$F_R = 4(\rho k_p)T^4 - 2\pi \int_0^\infty (\rho k_\nu) \left[\int_0^{t_\Delta} B_\nu E_1(|\tau_\nu - t_\nu|) dt_\nu - 2r_w E_2(\tau_\nu) \int_0^{t_\Delta} B_\nu E_2(t_\nu) dt_\nu \right] d\nu \tag{C3}$$

where r_w is the constant coefficient of reflection of the wall and t_ν a dummy variable of integration.

In the present report $r_w = 0$, and the absorption coefficient, discussed in appendix D, is approximated by a step function model with one to nine spectral steps. The value of the absorption coefficient is invariant within spectral range of each step but is allowed to change with temperature and density. Under these assumptions equation (C3) may be written as

$$F_R = 4(\rho k_p)T^4 - 2\pi \sum_{i=1}^{N} \int_{\Delta\nu_i} (\rho k_i) \left[\int_0^{t_{\Delta,i}} B_\nu E_1(|\tau_i - t_i|) dt_i \right] d\nu \tag{C4}$$

where N is the number of spectral steps considered. Since ρk_i is constant over $\Delta\nu_i$ it may be removed from under the integral and the integrations over ν and t, the optical thickness, transposed. Equation (C4) then becomes

$$F_R = 4(\rho k_p)T^4 - 2\sum_{i=1}^{N}(\rho k_i)\int_0^{t_{\Delta,i}} T^{*4} E_1(|\tau_i - t_i|)dt_i \tag{C5}$$

where

$$T^{*4} \equiv \eta_i T^4 \tag{C6}$$

and

$$\eta_i = \frac{\int_{\Delta\nu_i} B_\nu \, d\nu}{T^4/\pi} \tag{C7}$$

The problem, with flow properties being known across the stagnation line, is now reduced to the numerical evaluation of the integral

$$\int_0^{t_{\Delta,i}} T^{*4} E_1(|\tau_i - t_i|)dt_i \tag{C8}$$

for each spectral step in the absorption coefficient model. The optical thickness τ given by the integral

$$\tau_i = \int_0^{\Delta}(\rho k_i)dy \tag{C9}$$

is evaluated with the aid of closed Adams quadrature formulas. Hence the integral of equation (C8) is determinant at each point of the shock layer. With $dT^{*4}/d\tau$ evaluated as a local constant, equation (C8) integrated by parts, and the result substituted in equation (C5), the following expression for the divergence of the radiation flux vector at the kth mesh point results:

$$F_{R,k} = 4(\rho k_p)_k T_k^4 - 2\sum_{i=1}^{N}(\rho k_i)_k \Bigg(2T_{i,k}^{*4} - T_{i,1}^{*4} E_2(\tau_{i,k}) - (T_{i,M+1}^*)^4 E_2(|\tau_{i,M+1} - \tau_{i,k}|) - \sum_{j=1}^{M}\left\{\frac{(T_{i,j+1}^*)^4 - (T_{i,j}^*)^4}{\Delta t_i}\left[E_3(|t_{i,j+1} - \tau_{i,k}|) - E_3(|t_{i,j} - \tau_{i,k}|)\right]\right\}\Bigg) \tag{C10}$$

with

$$\Delta t_i = \tau_{i,j+1} - \tau_{i,j} \tag{C11}$$

where the shock layer contains $M + 1$ mesh points.

A considerable saving in computing time and computer storage requirements can be effected if the shock layer is divided into equal increments of the optical thickness rather than Y. This division is carried out for each spectral step with third-order Lagrangian extrapolation polynomials used to obtain flow quantities at the resulting mesh points. The quantity Δt_i now becomes

$$\Delta t_i = \frac{\tau_{i,M+1}}{M} \tag{C12}$$

For purposes of accuracy, a finer mesh is used in the calculation of $F_{R,k}$ than is used in the general flow-field calculation.

APPENDIX D

STEP MODEL ABSORPTION COEFFICIENT

The absorption coefficient models used in this report are either identical to, or derived from, the model absorption coefficient reported by Olstad (ref. 8). In reference 8, Olstad presents data, tabulated for a range of temperatures and densities for each step of a nine-step model of the absorption coefficient. This information, for purposes of reference is presented herein as table I. Included in this absorption coefficient model are contributions due to atomic line transitions, N^+- and O^+-electron recombination, free-free transitions, and molecular bond transitions. Equilibrium air properties are assumed to exist.

The absorption due to line radiation in the wavelength interval 911 to 1800 Å was determined with the aid of parameters presented by Griem (ref. 11). In order to incorporate the resultant absorption coefficient information realistically into a step model, Olstad developed a "picket fence" model in which the line information is represented by a large number of narrow (in wavelength) steps of height $\alpha_1(\rho,T)$ superposed on a gray background of height $\alpha_2(\rho,T)$. The relative width and spacing of the steps are taken into account by a parameter $\beta(\rho,T)$. Sketch D1 illustrates Olstad's model for line radiation between 911 and 1800 Å.

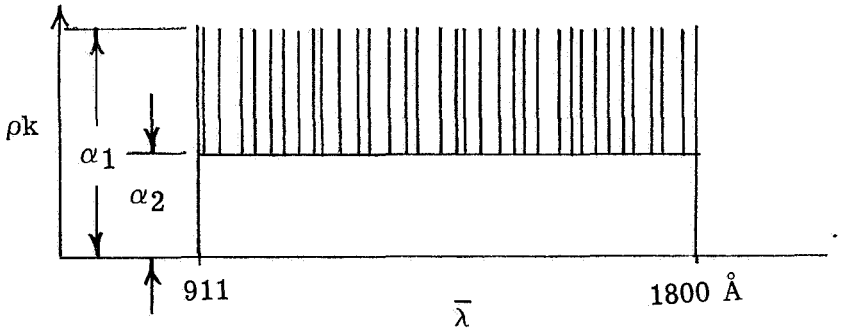

Sketch D1

A detailed discussion of the model, its restrictions, and the means by which the governing parameters α_1, α_2, and β are determined are presented in reference 8. It suffices here to say that this model appears to be a reasonable means of treating the absorption coefficient due to line radiation where the lines may not be optically thin. Above 1800 Å, contributions to the absorption coefficient, including line radiation, are treated as optically thin and are represented by a Planck average. In fact, for some of the larger nose radii, the line centers may be optically thick not thin. The spectral distribution of the black body function coupled with arguments in the section "Results and

Discussion" (regarding the relative contributions of line centers and line wings) indicate that the resulting heat-transfer error will be small.

In the vacuum ultraviolet, contributions to the absorption of radiation due to N^+- and O^+-electron recombination were obtained from Hahne (ref. 17). Of the twelve photo-ionization edges indicated by Hahne, four were used in the construction of the step model absorption coefficient presented in reference 8. These edges are located at wavelengths of 852, 911, 1020, and 1130 Å. No contributions to the absorption coefficient are included below 400 Å.

Absorption coefficient models used in this report include a gray, a two-step, a three-step, and a nine-step model. The nine-step model is used directly as presented in table I. The other models are constructed from the nine-step model by means of Planck averages of various combinations of steps and are summarized in table II.

It should be noted that all absorption models are constructed from the same basic spectral information and hence are consistent. This allows meaningful comparisons of flow profiles and heat-transfer solutions to be made between models of varying spectral complexity.

REFERENCES

1. Howe, John T.; and Viegas, John R.: Solutions of the Ionized Radiating Shock Layer, Including Reabsorption and Foreign Species Effects, and Stagnation Region Heat Transfer. NASA TR R-159, 1963.

2. Hoshizaki, H.; and Wilson, K. H.: Convective and Radiative Heat Transfer During Superorbital Entry. NASA CR-584, 1966.

3. Olstad, Walter B.: Stagnation-Point Solutions for Inviscid, Radiating Shock Layers. Ph.D. Thesis, Harvard Univ., 1966.

4. Anderson, John D., Jr.: Nongray Radiative Transfer Effects on the Radiating Stagnation Region Shock Layer and Stagnation Point Heat Transfer. NOLTR 67-104, U.S. Navy, July 10, 1967. (Available from DDC as AD658321.)

5. Moretti, Gino; and Abbett, Michael: A Time-Dependent Computational Method for Blunt Body Flows. AIAA J., vol. 4, no. 12, Dec. 1966, pp. 2136-2141.

6. Lax, Peter D.: Weak Solutions of Nonlinear Hyperbolic Equations and Their Numerical Computation. Commun. Pure Appl. Math., vol. VII, no. 1, Feb. 1954, pp. 159-193.

7. Lax, Peter D.; and Wendroff, Burton: Difference Schemes for Hyperbolic Equations With High Order of Accuracy. Commun. Pure Appl. Math., vol. XVII, no. 3, Aug. 1964, pp. 381-398.

8. Olstad, Walter B.: Blunt-Body Stagnation-Region Flow With Nongray Radiation Heat Transfer – A Singular Perturbation Solution. NASA TR R-295, 1968.

9. Cohen, Nathaniel B.: Correlation Formulas and Tables of Density and Some Transport Properties of Equilibrium Dissociating Air for Use in Solutions of the Boundary-Layer Equations. NASA TN D-194, 1960.

10. Cohen, Nathaniel B.: Boundary-Layer Similar Solutions and Correlation Equations for Laminar Heat-Transfer Distribution in Equilibrium Air at Velocities up to 41,000 Feet Per Second. NASA TR R-118, 1961.

11. Griem, Hans R.: Plasma Spectroscopy. McGraw-Hill Book Co., c.1964.

12. Wilson, K. H.; and Hoshizaki, H.: A Study of Superorbital Heating Problems. Volume 1 – Effect of Ablation Product Absorption and Line Transitions on Shock Layer Radiative Transport. 4-17-67-11, Vol. I, Lockheed Missiles & Space Co., July 1968.

13. Chin, Jin H.: Radiation Transport for Stagnation Flows Including the Effect of Lines and Ablation Layer. AIAA Paper No. 68-664, June 1968.

14. Page, William A.; Compton, Dale L.; Borucki, William J.; Ciffone, Donald L.; and Cooper, David M.: Radiative Transport in Inviscid Nonadiabatic Stagnation-Region Shock Layers. AIAA Paper No. 68-784, June 1968.

15. Rigdon, W. S.; Dirling, R. B., Jr.; and Thomas, M.: Radiative and Convective Heating During Atmospheric Entry. NASA CR-1170, 1968.

16. Moretti, Gino: Three-Dimensional Flow Field Analysis in Re-Entry Problems. Re-Entry. Vol. IV of Ballistic Missile and Aerospace Technology, C. T. Morrow, L. D. Ely, and M. R. Smith, eds., Academic Press, 1961, pp. 89-109.

17. Hahne, Gerhard E.: The Vacuum Ultraviolet Radiation From N^+- and O^+-Electron Recombination in High-Temperature Air. NASA TN D-2794, 1965.

TABLE I.- NINE-STEP-MODEL ABSORPTION COEFFICIENT

[Final numbers listed with values of ρk_1, ρk_2, etc., represent powers of 10; for example, 5.001+1 signifies 5.001×10]

Wavelength interval		400 to 852 Å	852 to 911 Å	911 to 1020 Å	911 to 1020 Å	1020 to 1130 Å	1020 to 1130 Å	1130 to 1800 Å	1130 to 1800 Å	1800 Å to ∞
$\overline{T}$, °K	$\overline{\rho}/\overline{\rho}_0$	$\overline{\rho k_1}$, m^{-1}	$\overline{\rho k_2}$, m^{-1}	$\overline{\rho k_3}$, m^{-1}	$\overline{\rho k_4}$, m^{-1}	$\overline{\rho k_5}$, m^{-1}	$\overline{\rho k_6}$, m^{-1}	$\overline{\rho k_7}$, m^{-1}	$\overline{\rho k_8}$, m^{-1}	$\overline{\rho k_9}$, m^{-1}
8 000	10^{-3}	5.001+1	8.629+0	2.786+0	8.360+1	3.457-1	8.115+1	3.404-3	8.082+1	4.285-4
10 000	↓	4.606+1	1.067+1	5.012+0	2.464+2	8.511-1	2.422+2	2.443-2	2.414+2	4.571-3
12 000	↓	3.319+1	1.004+1	5.433+0	1.601+2	1.132+0	1.588+2	5.470-2	1.547+2	1.690-2
14 000	↓	1.577+1	5.902+0	3.350+0	9.039+1	8.091-1	8.784+1	6.152-2	8.710+1	2.786-2
16 000	↓	5.297+0	2.291+0	1.355+0	4.229+1	3.681-1	4.100+1	3.945-2	4.094+1	2.564-2
8 000	10^{-2}	4.678+2	8.418+1	2.583+1	3.165+2	3.214+0	2.939+2	2.570-2	2.907+2	8.318-3
10 000	↓	4.880+2	1.123+2	5.304+1	3.029+2	8.913+0	2.588+2	1.242-1	2.500+2	4.943-2
12 000	↓	4.389+2	1.294+2	7.241+1	2.853+2	1.475+1	2.276+2	3.236-1	2.132+2	2.415-1
14 000	↓	3.370+2	1.212+2	7.295+1	2.502+2	1.702+1	1.943+2	5.483-1	1.778+2	7.194-1
16 000	↓	2.107+2	8.833+1	5.480+1	1.923+2	1.417+1	1.516+2	6.546-1	1.381+2	1.002+0
8 000	10^{-1}	3.296+3	7.394+2	1.717+2	4.628+2	2.123+1	3.124+2	1.148-1	2.912+2	2.254-1
10 000	↓	4.764+3	1.112+3	5.153+2	7.941+2	8.553+1	3.648+2	5.888-1	2.793+2	6.887-1
12 000	↓	4.775+3	1.393+3	7.881+2	1.050+3	1.590+2	4.206+2	1.507+0	2.631+2	2.793+0
14 000	↓	4.375+3	1.545+3	9.548+2	1.189+3	2.192+2	4.529+2	2.594+0	2.363+2	8.531+0
16 000	↓	3.715+3	1.517+3	9.820+2	1.189+3	2.477+2	4.543+2	3.412+0	2.100+2	1.745+1
Type of contribution		(a)	(a)	(a)	(b)	(a)	(b)	(a)	(b)	(c)

[a]Absorption due to free-free and free-bound interactions and due to line wings.

[b]Absorption due to line steps, free-free, and free-bound interactions.

[c]All absorption effects.

TABLE II.- SUMMARY OF STEP-MODEL ABSORPTION COEFFICIENT

Model	Step	Wavelength interval, Å	Formed from Planck average of these steps of table I
Gray	1	400 to 100 000	1 to 9
Two step	1	400 to 1 130	1 to 6
	2	1 130 to 100 000	7 to 9
Three step model A	1	400 to 1 130	1 to 6
	2	1 130 to 1 800	8
	3	1 130 to 100 000	7 and 9
Nine step	The nine-step model is used as it appears in table I		

TABLE III.- SUMMARY OF MOLE FRACTIONS OF SELECTED AIR SPECIES AT SHOCK WAVE AND BODY FOR $\overline{V}_\infty$ = 15 240 m/s, $\overline{\rho}_\infty/\overline{\rho}_0 = 10^{-4}$, and $\overline{R}_N$ = 1 m

Species	Mole fraction	
	Shock wave ($\overline{T}$ = 13 750 °K; $\overline{p}$ = 0.264 atm)	Body ($\overline{T}$ = 8 700 °K; $\overline{p}$ = 0.275 atm)
E^-	3.52×10^{-1}	1.14×10^{-2}
N	2.24×10^{-1}	7.81×10^{-1}
N^+	2.97×10^{-1}	9.66×10^{-3}
0	7.00×10^{-2}	1.87×10^{-1}
0^+	5.31×10^{-2}	1.66×10^{-3}
N2	1.75×10^{-6}	5.13×10^{-3}
$N2^+$	2.28×10^{-6}	2.56×10^{-5}
02	7.68×10^{-9}	8.33×10^{-7}
02^+	3.78×10^{-8}	1.10×10^{-7}
02^-	2.35×10^{-13}	3.88×10^{-12}
N0	2.00×10^{-7}	7.81×10^{-5}
$N0^+$	2.54×10^{-6}	9.47×10^{-5}

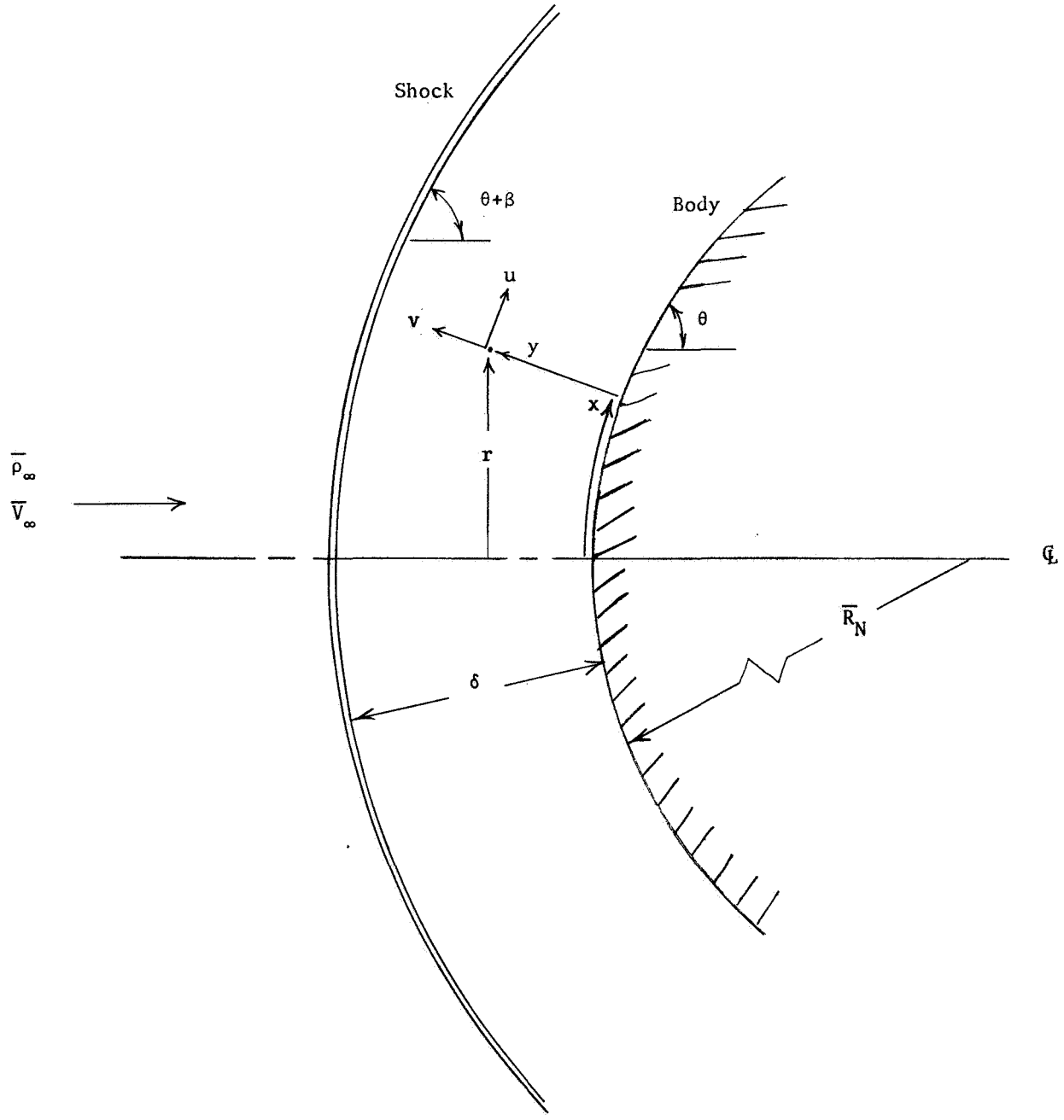

Figure 1.- Schematic of flow field and body-oriented coordinate system.

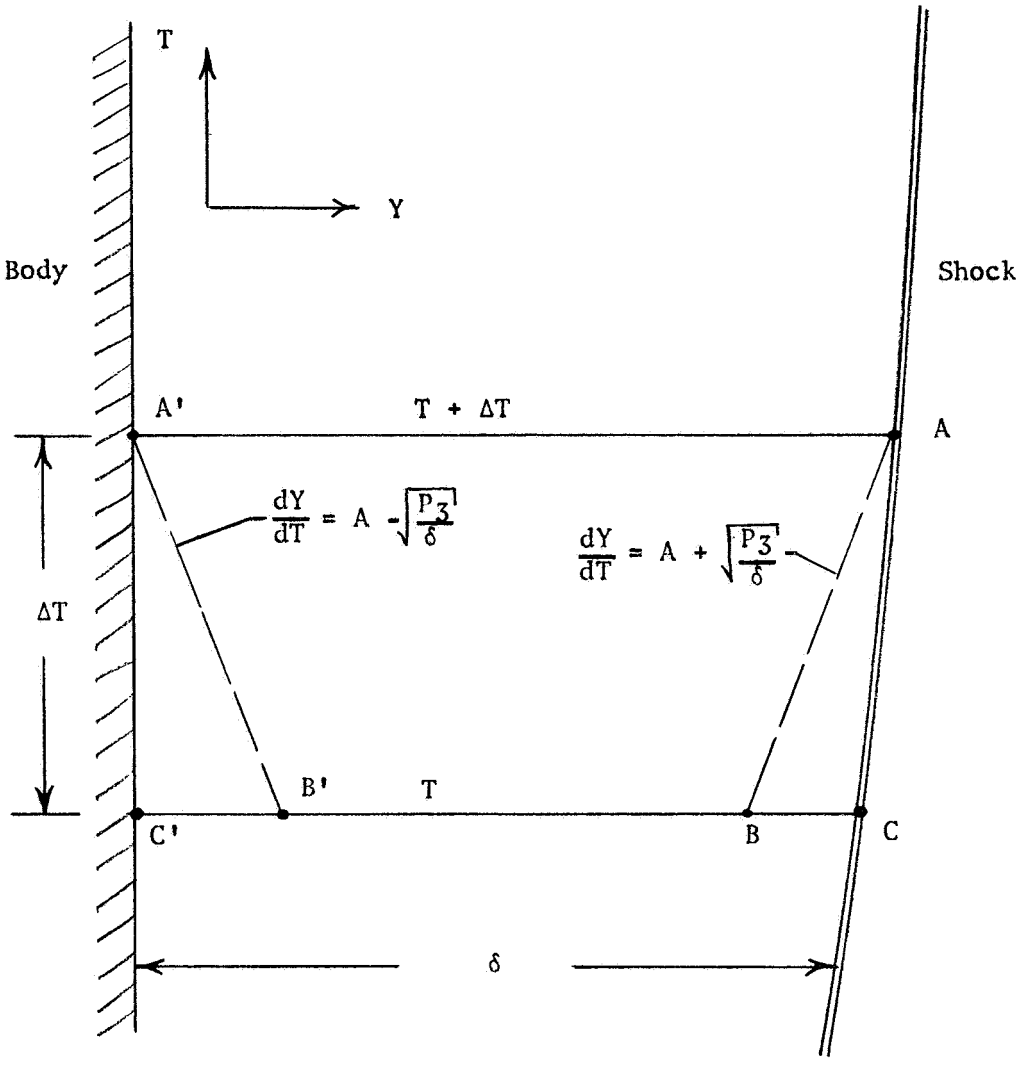

Figure 2.- Schematic of use of unsteady characteristics at shock wave and body.

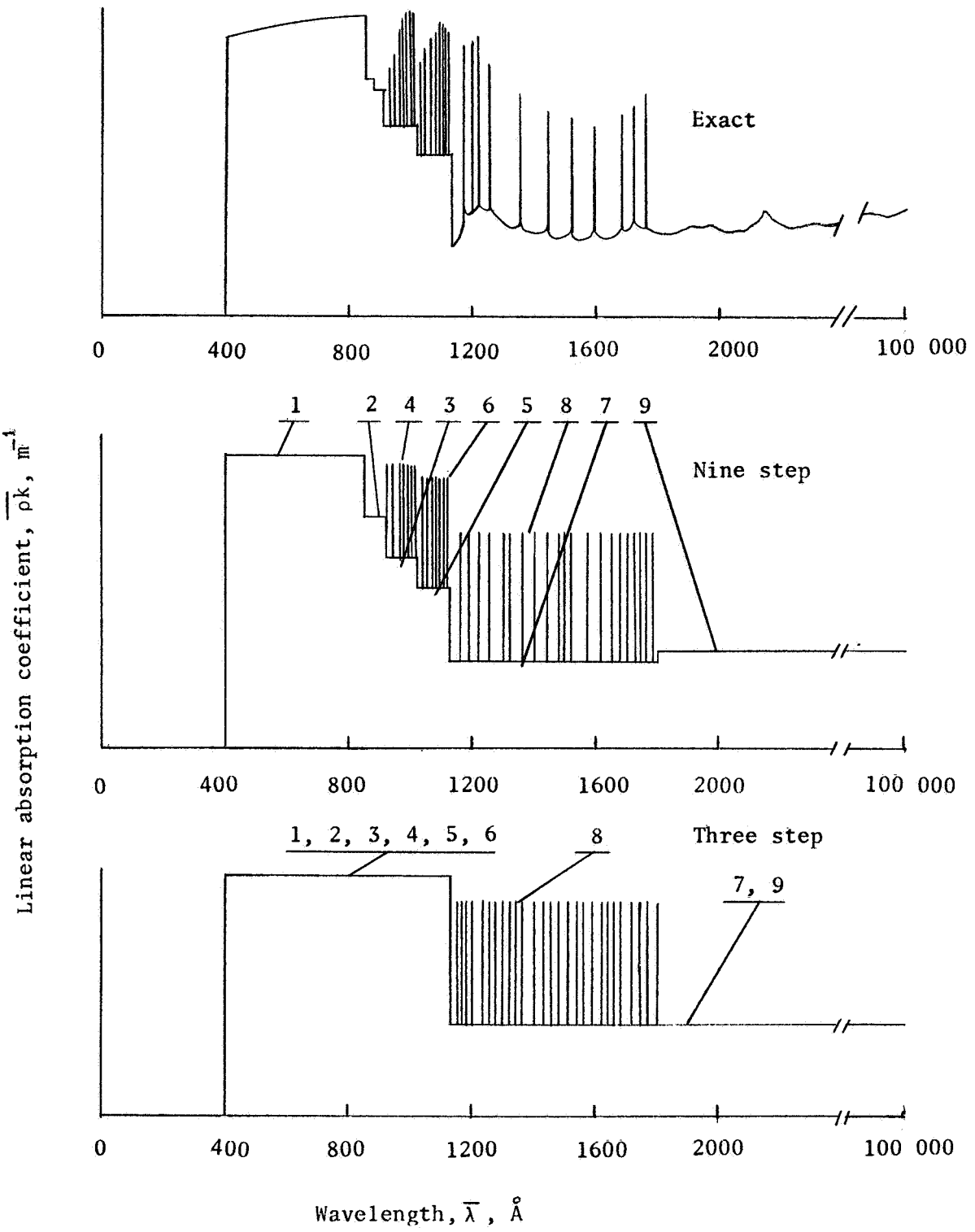

(a) Exact, nine-step, and three-step absorption coefficients.

Figure 3.- Schematic of absorption coefficient models.

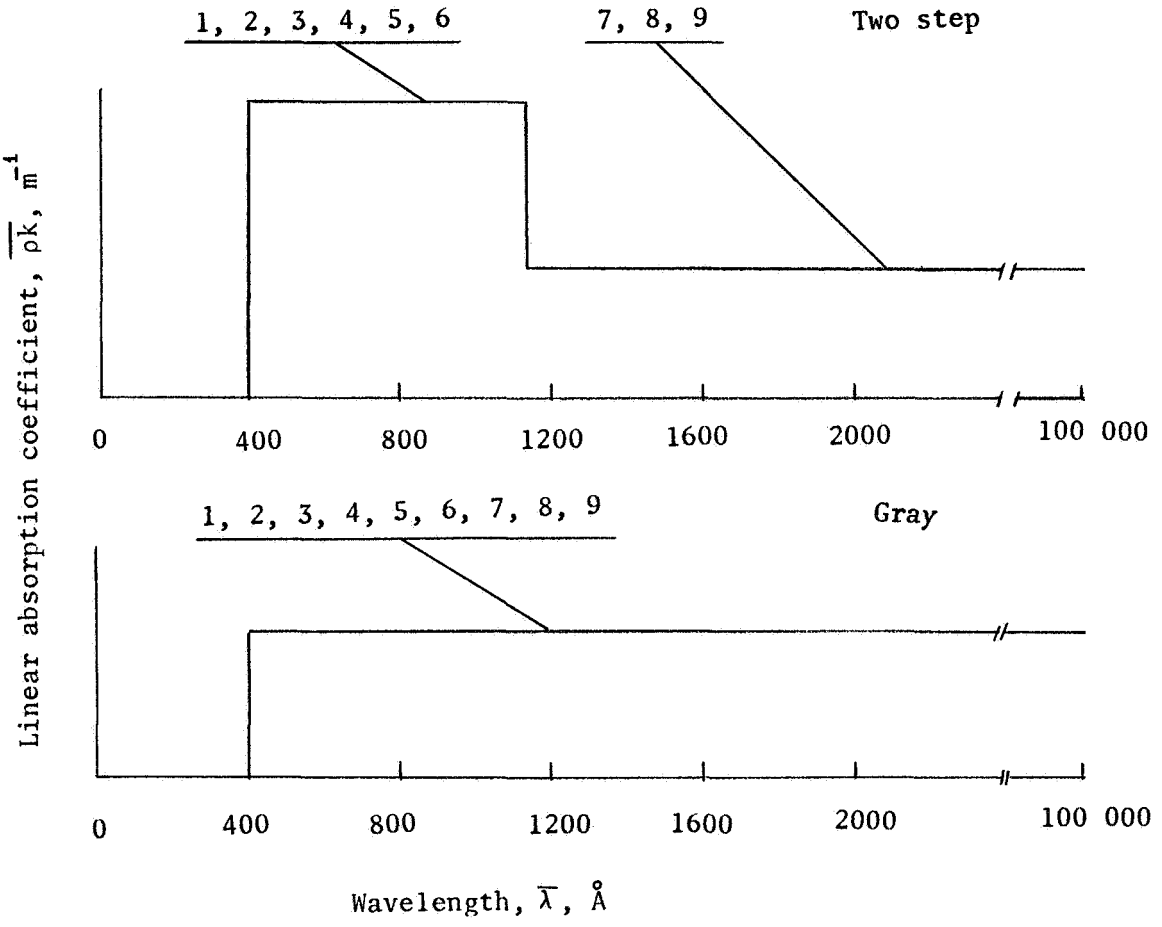

(b) Two-step and gray absorption coefficients.

Figure 3.- Concluded.

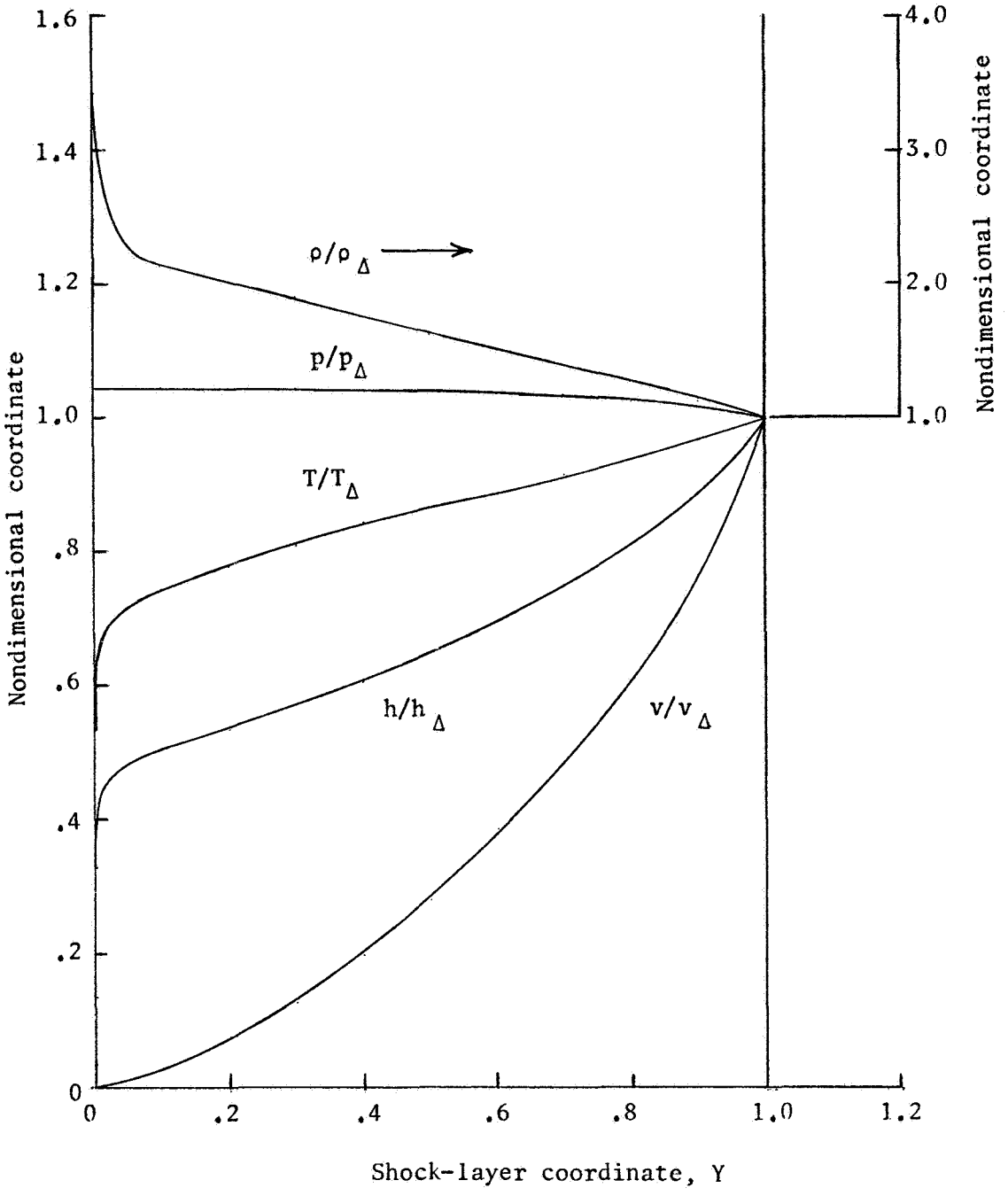

Figure 4.- Typical flow profiles. Nongray, nonadiabatic, absorbing flow; $\bar{V}_\infty$ = 14 000 m/s; $\bar{R}_N$ = 10 m; $\bar{\rho}_\infty/\bar{\rho}_0 = 10^{-4}$; three-step model.

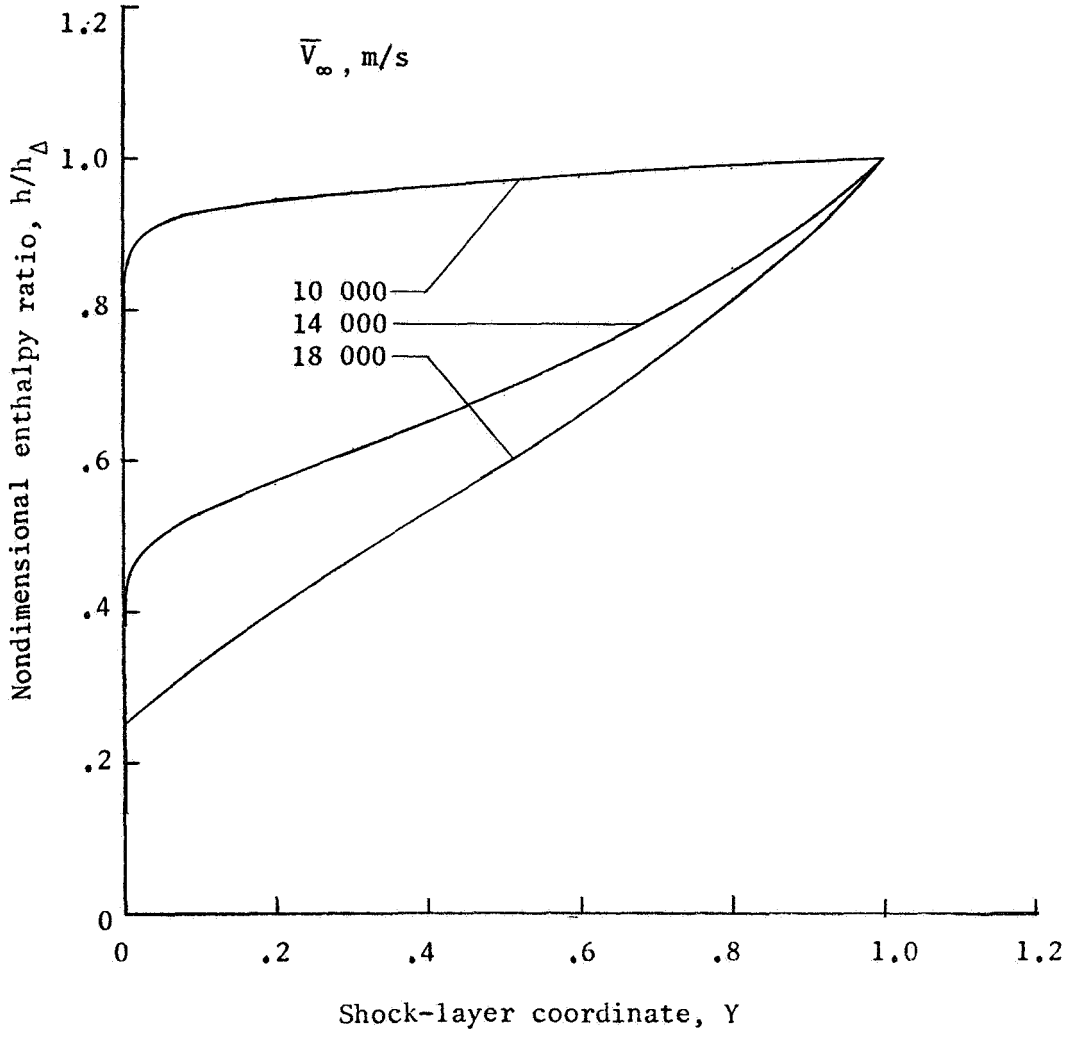

Figure 5.- Variation of enthalpy profile with $\bar{V}_\infty$. Nongray, nonadiabatic, absorbing flow; $\bar{R}_N$ = 2 m; $\bar{p}_\infty/\bar{p}_0 = 10^{-3}$; three-step model.

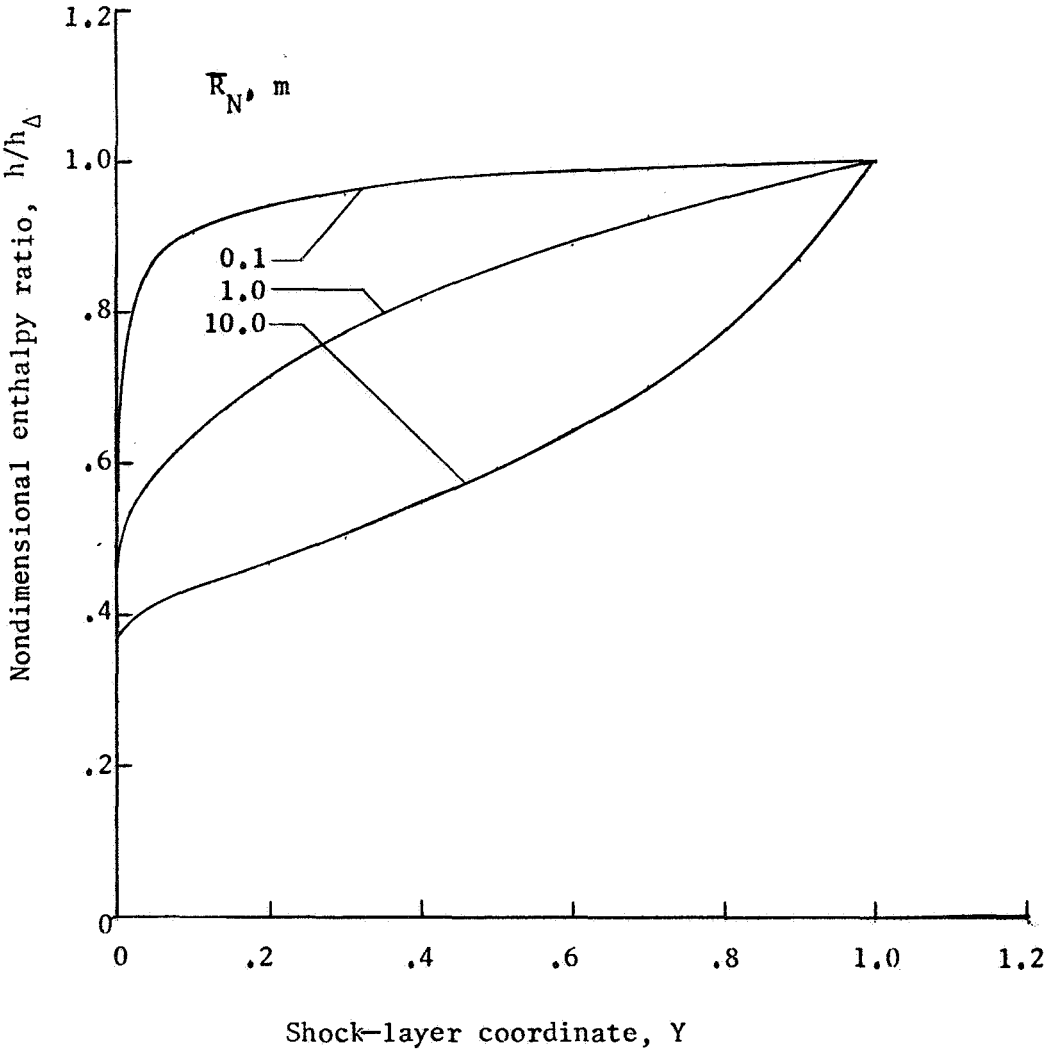

Figure 6.- Variation of enthalpy profile with $\bar{R}_N$. Nongray, nonadiabatic, absorbing flow; $\bar{V}_\infty$ = 15 240 m/s; $\bar{\rho}_\infty/\bar{p}_0 = 10^{-4}$; three-step model.

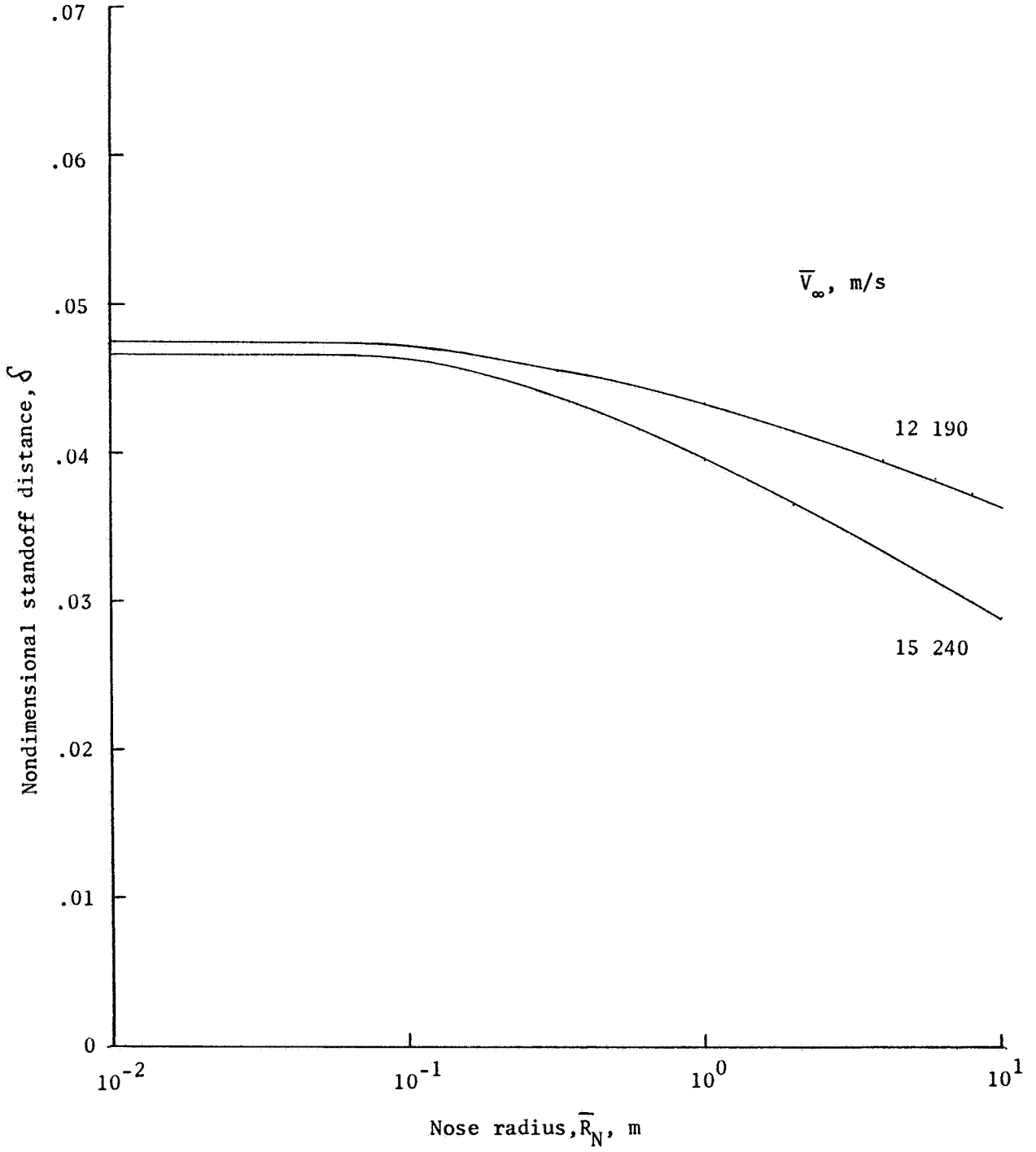

Figure 7.- Variation of standoff distance with velocity and nose radius. $\bar{p}_\infty/\bar{p}_0 = 10^{-4}$; three-step model.

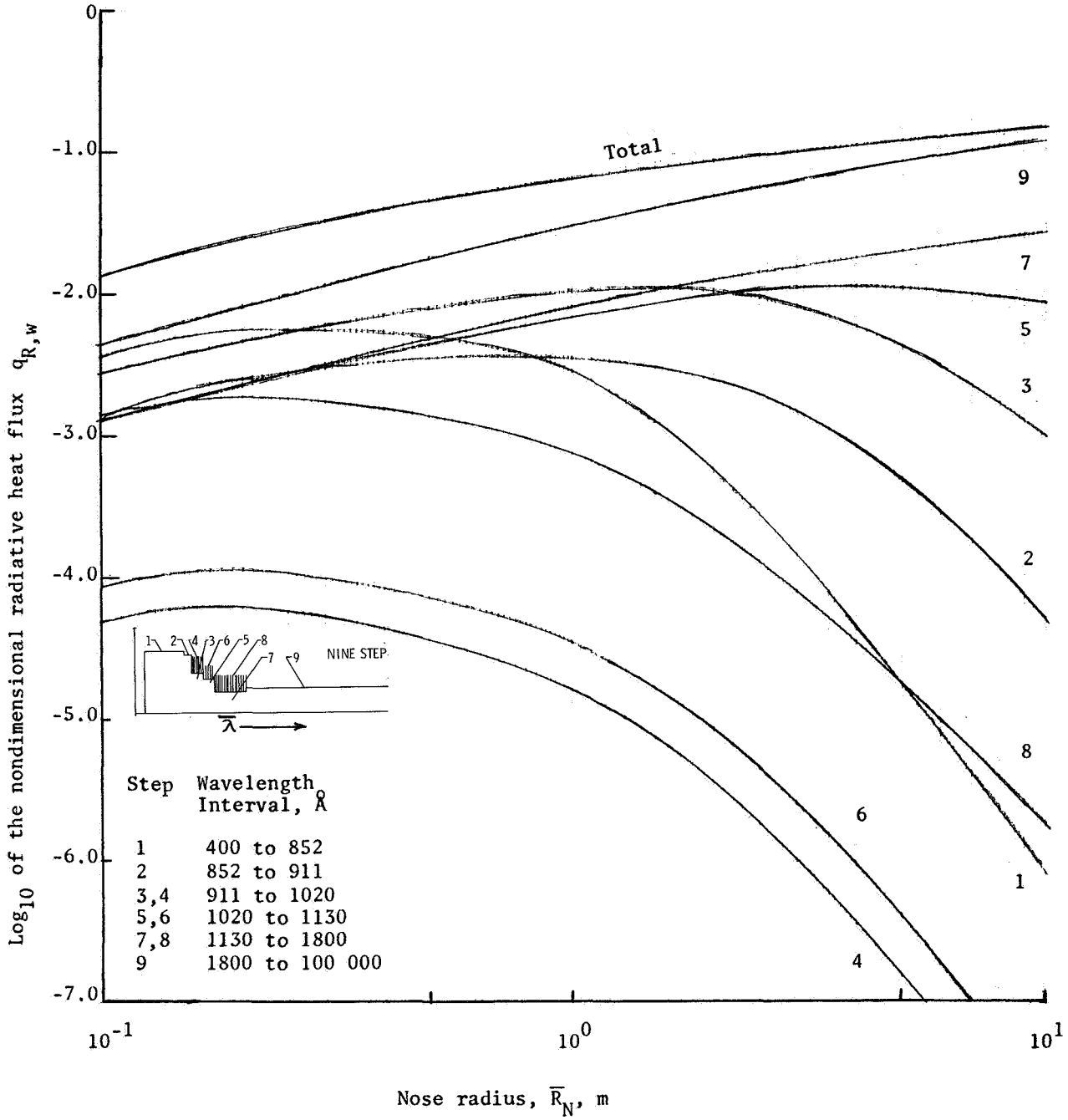

Figure 8.- Contribution of various spectral regions to total radiative heat transfer. $\bar{V}_\infty$ = 15 240 m/s; $\bar{\rho}_\infty/\bar{\rho}_0 = 10^{-4}$; nine-step-model absorption coefficient.

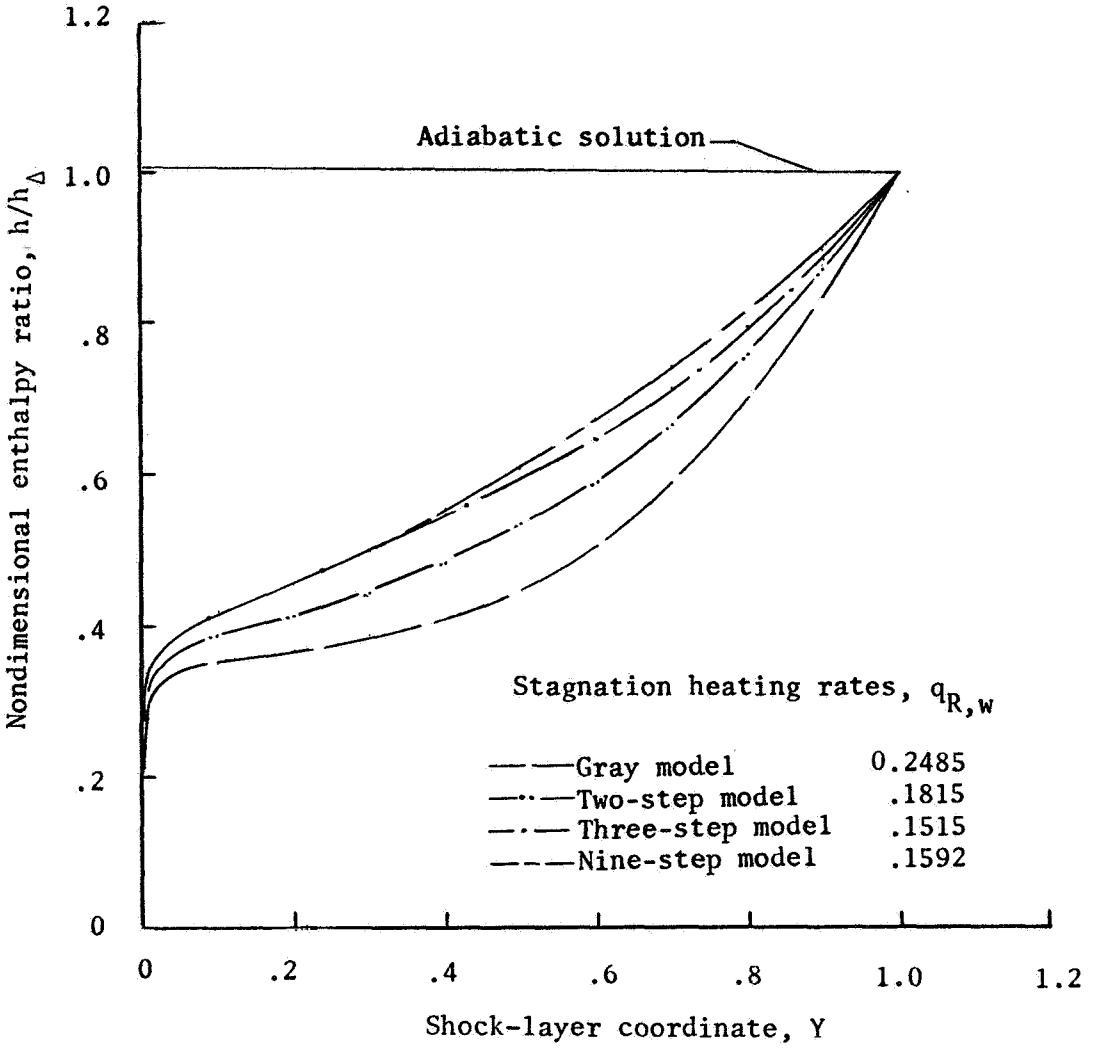

Figure 9.- Effect on enthalpy profile of step model variations. $\bar{V}_\infty$ = 16 000 m/s; $\bar{R}_N$ = 8.0 m; $\bar{p}_\infty/\bar{p}_0 = 10^{-4}$.

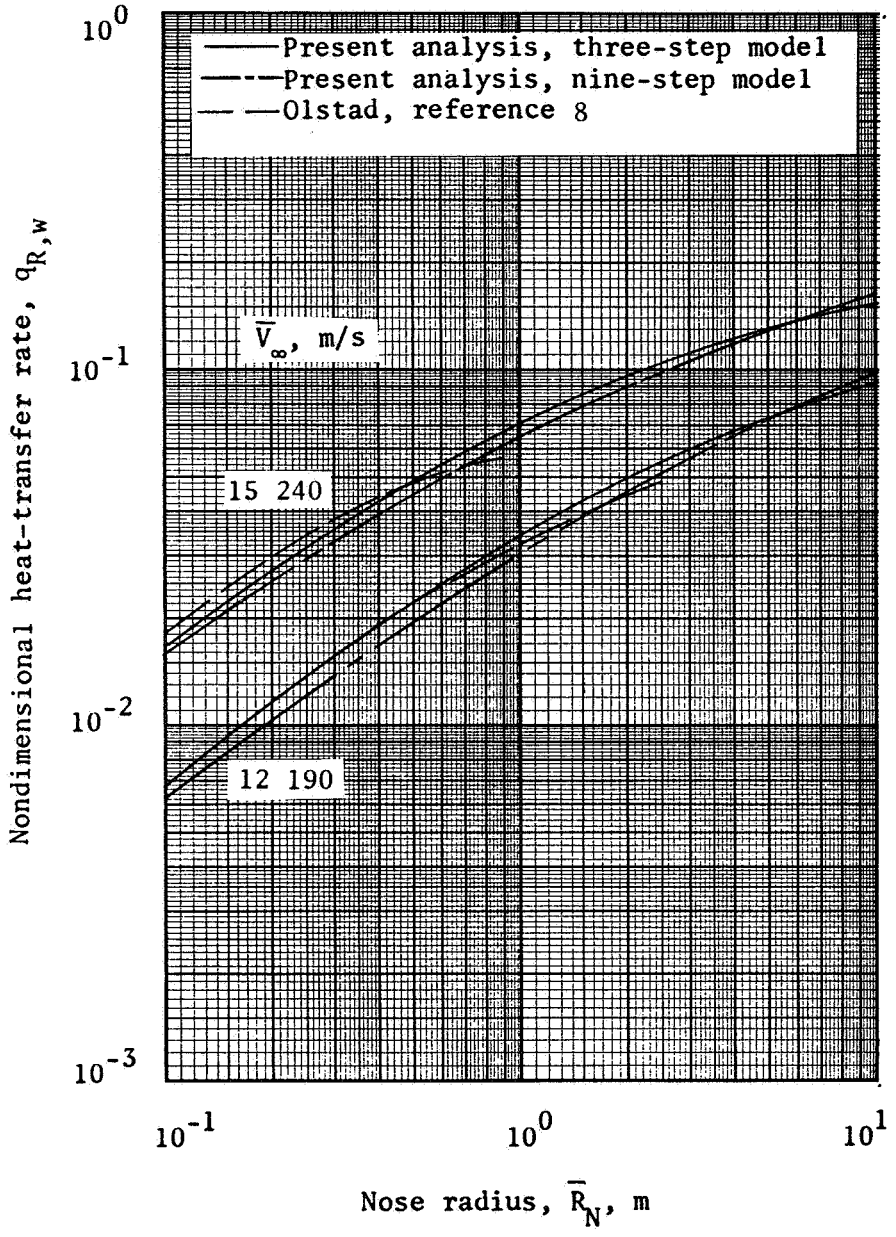

Figure 10.- Comparison of stagnation-point heat-transfer rates. $\bar{Z}$ = 67.06 km.

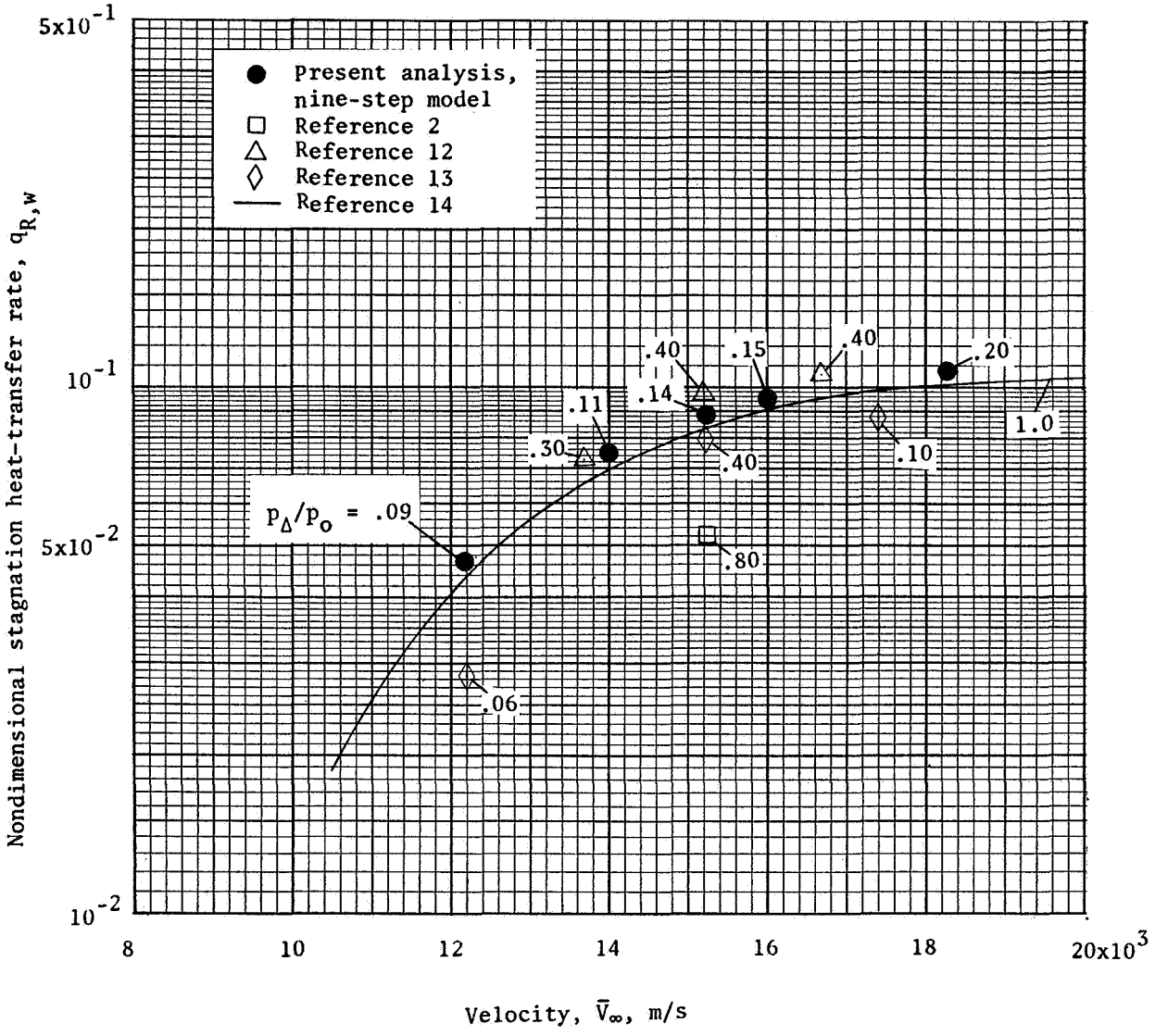

Figure 11.- Comparison of stagnation-point heat-transfer rates. $\bar{\delta}_a$ = 0.10 m.

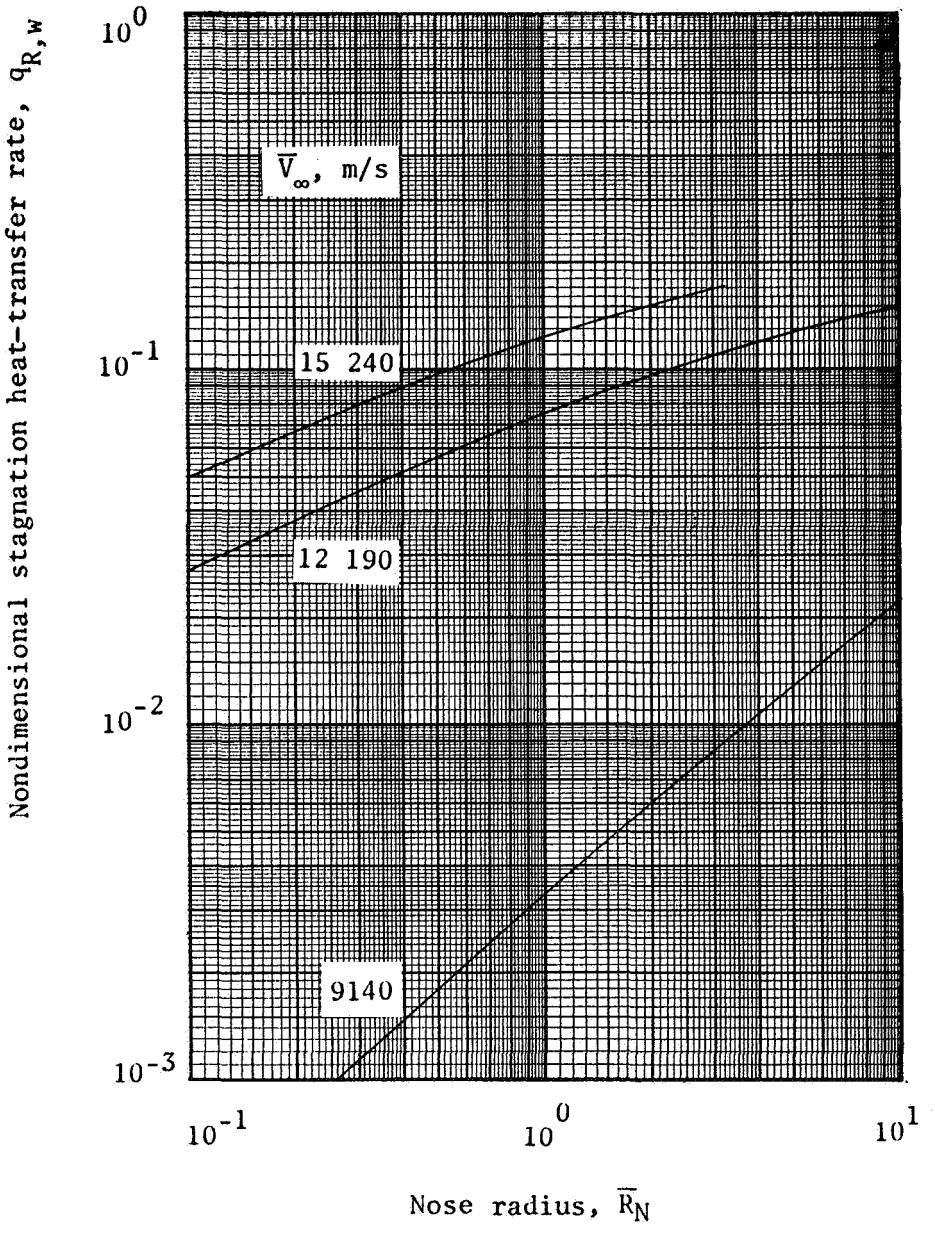

(a) $\bar{Z}$ = 42.67 km.

Figure 12.- Variation of $q_{R,W}$ with $\bar{R}_N$, $\bar{V}_\infty$, and $\bar{Z}$. Calculations carried out by using three-step model.

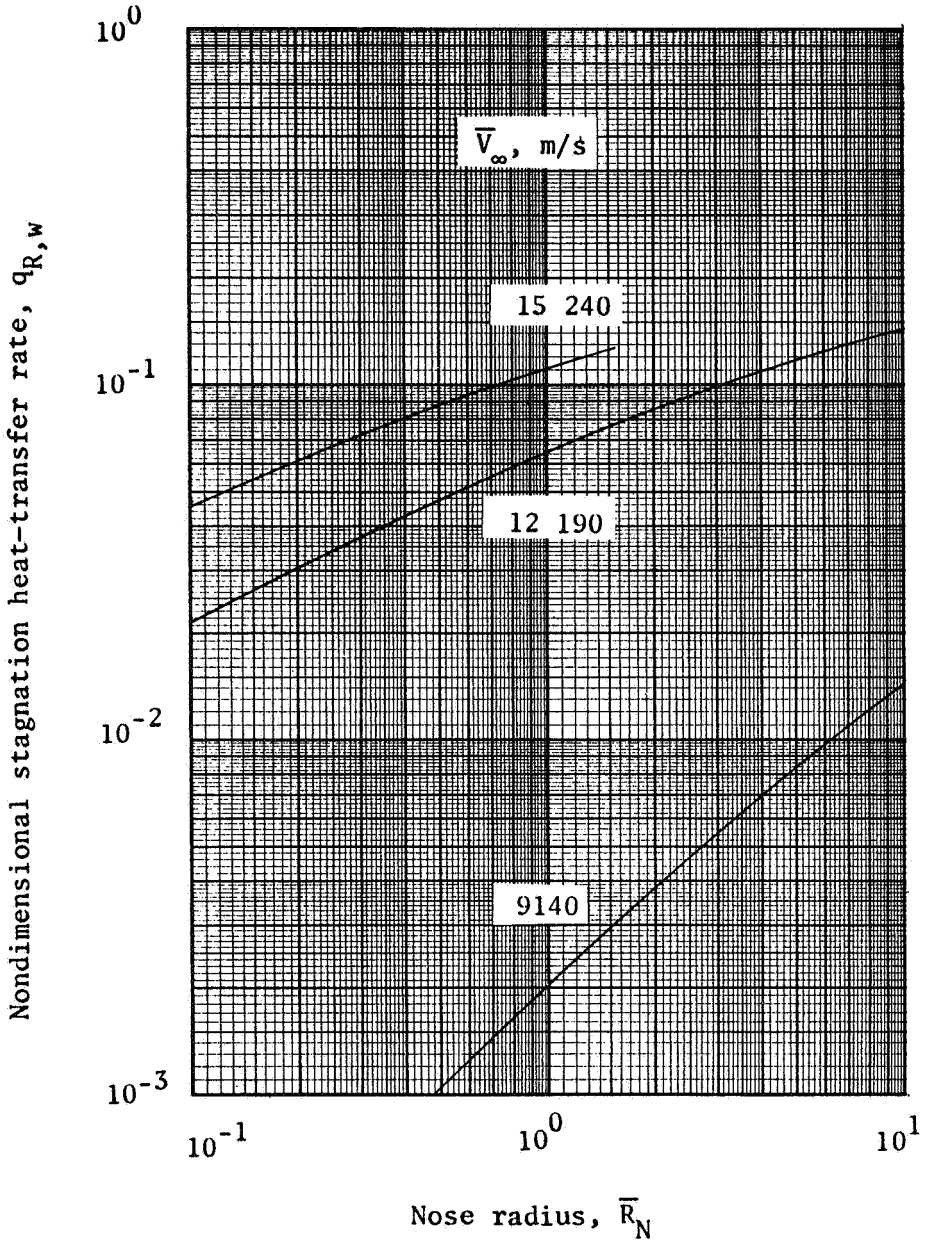

(b) $\overline{Z}$ = 48.77 km.

Figure 12.- Continued.

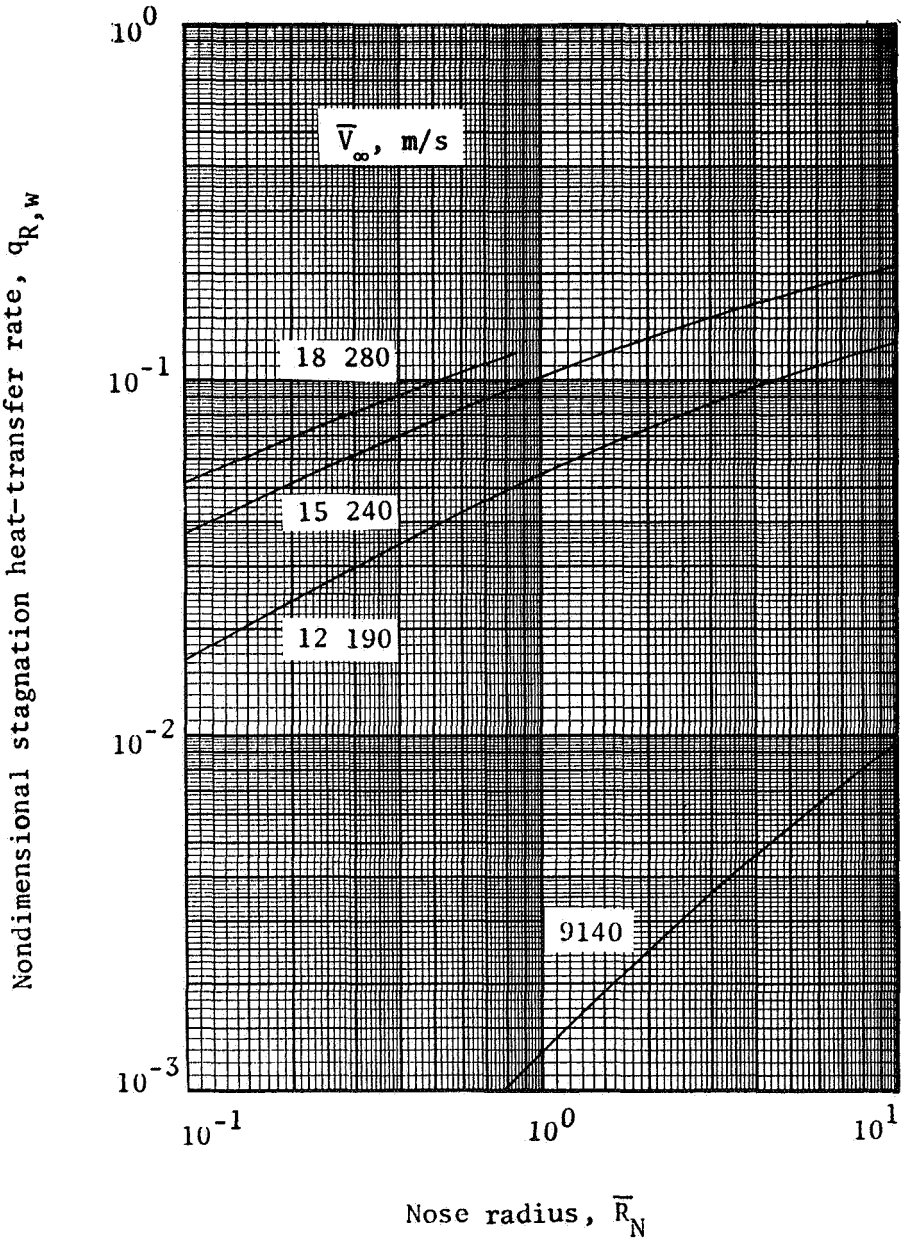

(c) $\bar{Z}$ = 54.86 km.

Figure 12.- Continued.

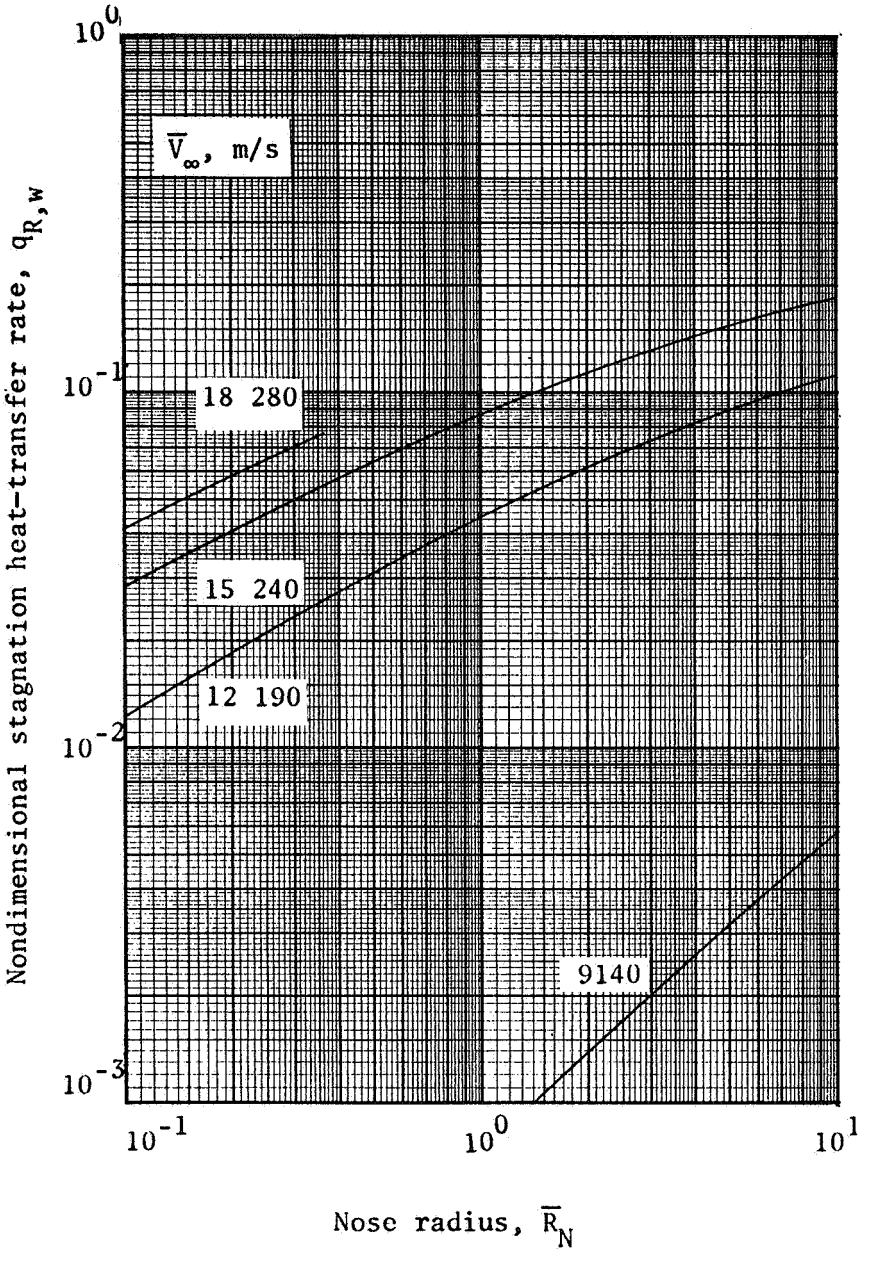

(d) $\overline{Z}$ = 60.96 km.

Figure 12.- Continued.

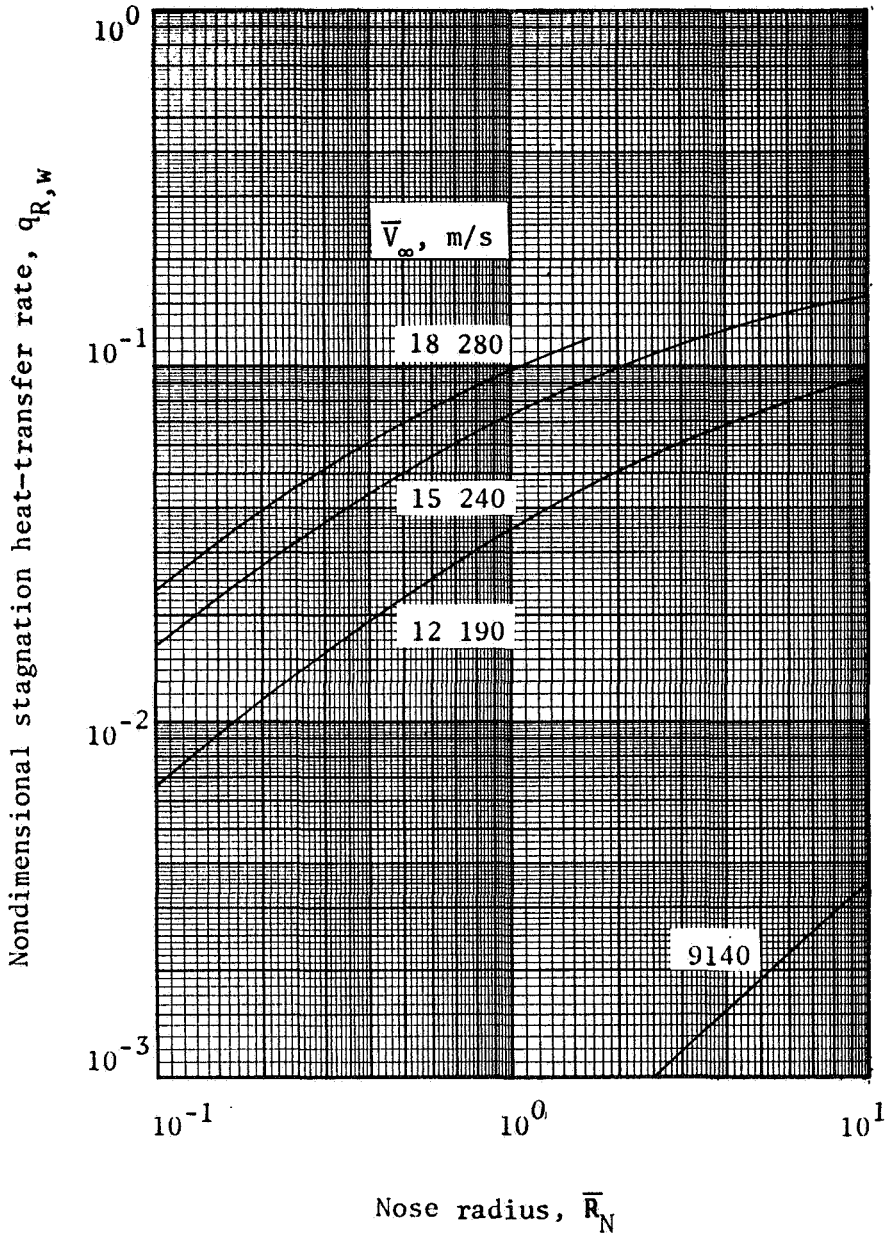

(e) $\bar{Z}$ = 67.06 km.

Figure 12.- Continued.

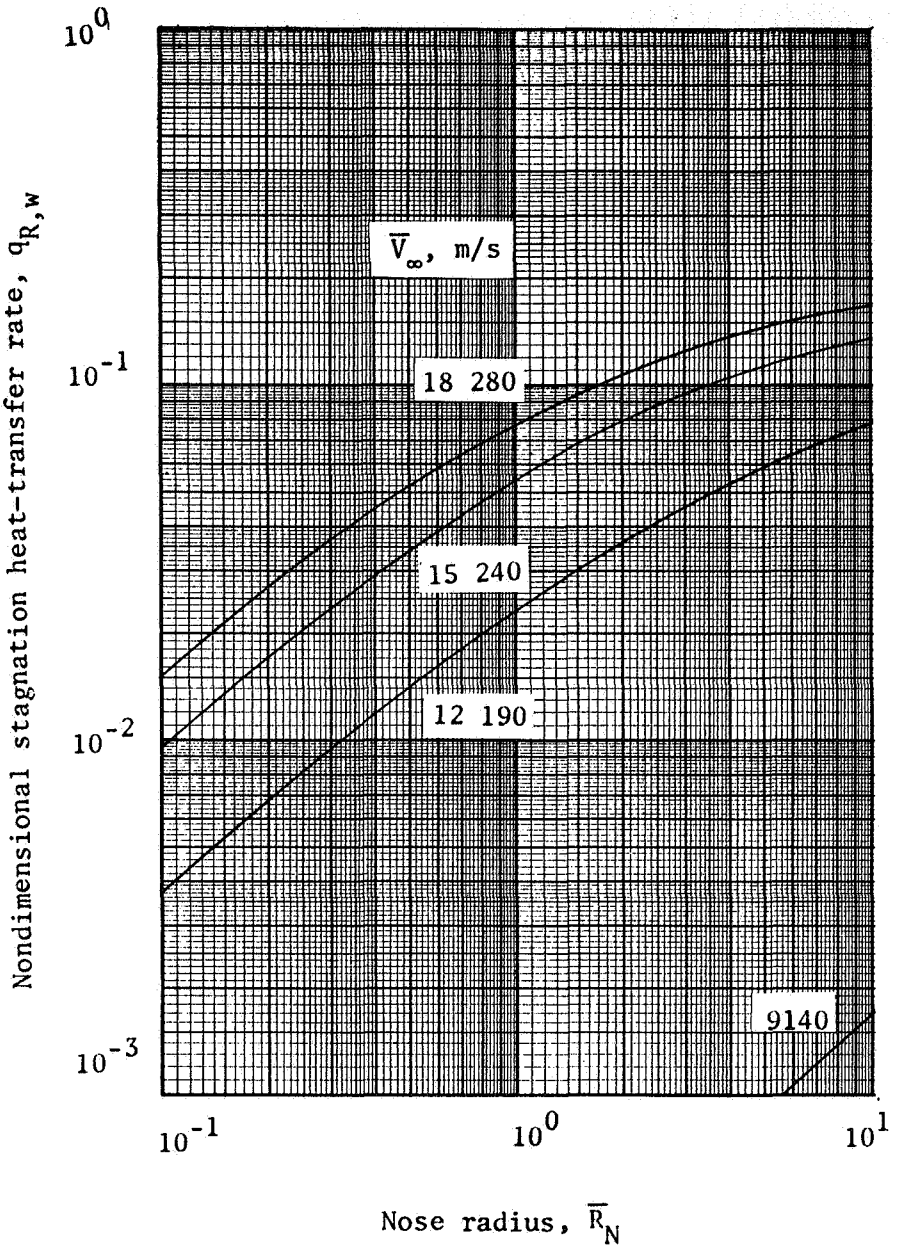

(f) $\overline{Z}$ = 73.15 km.

Figure 12.- Concluded.

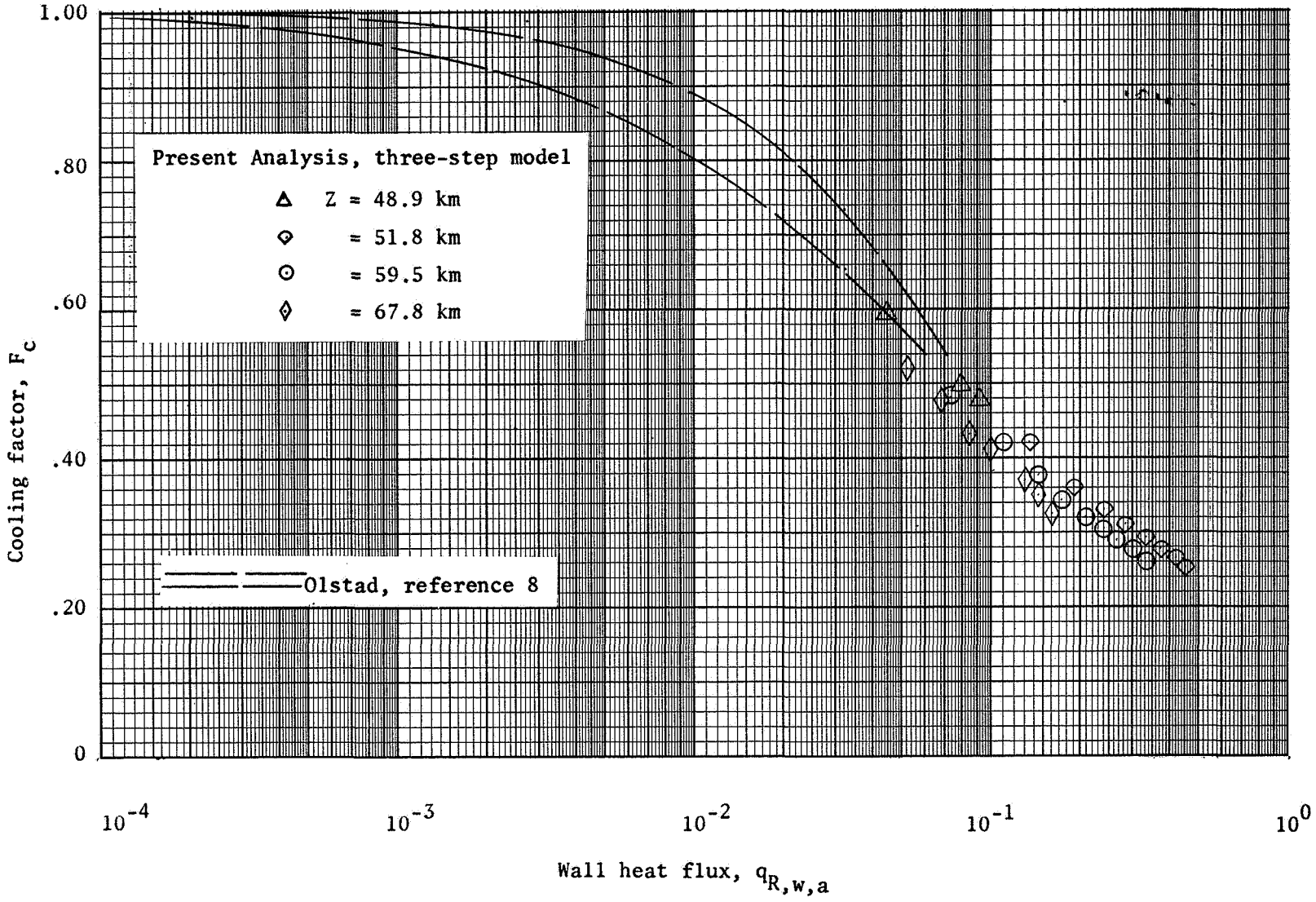

(a) $\overline{V}_\infty$ = 9140 m/s.

Figure 13.- Cooling-factor correlations.

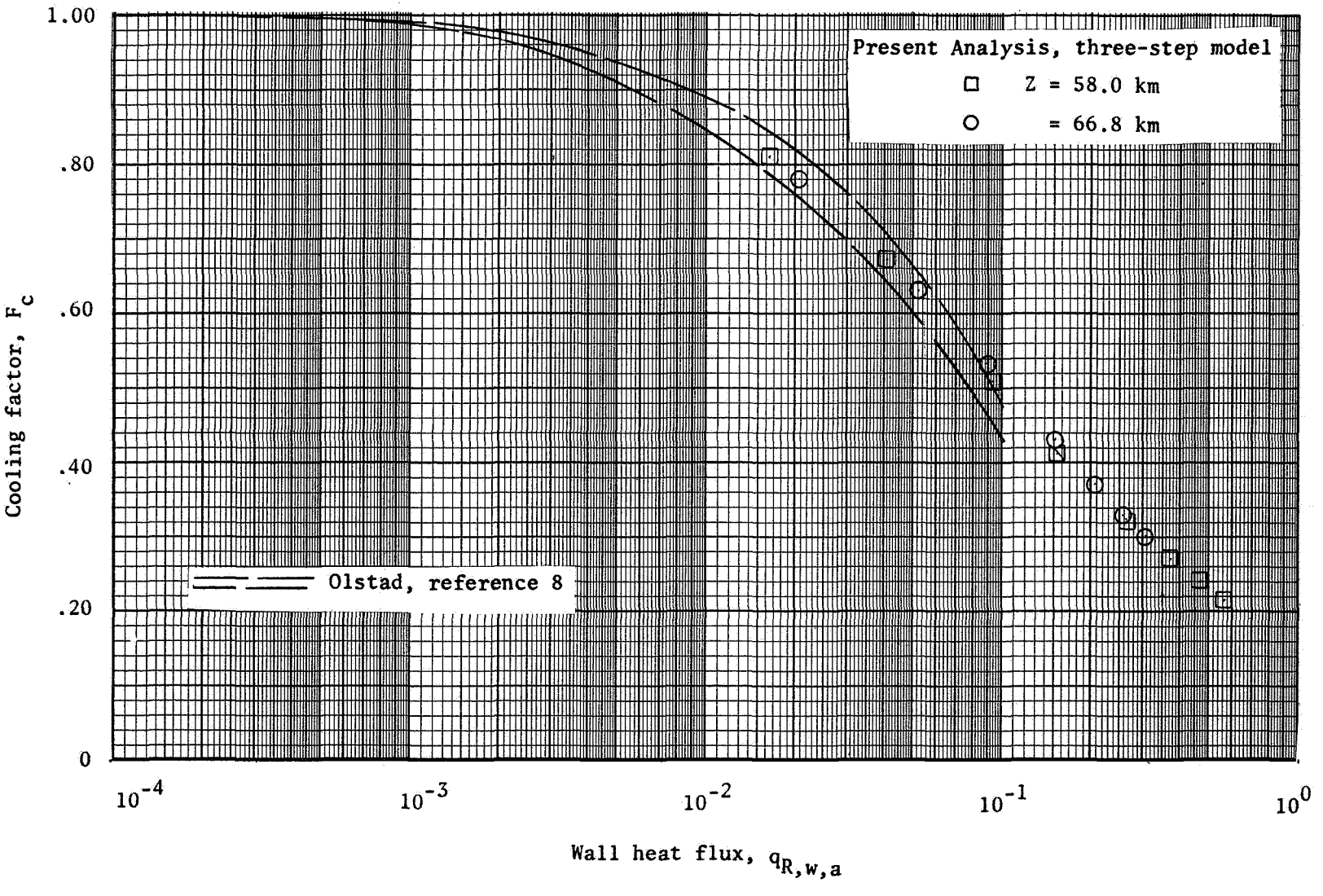

(b) $\bar{V}_\infty$ = 12 190 m/s.

Figure 13.- Continued.

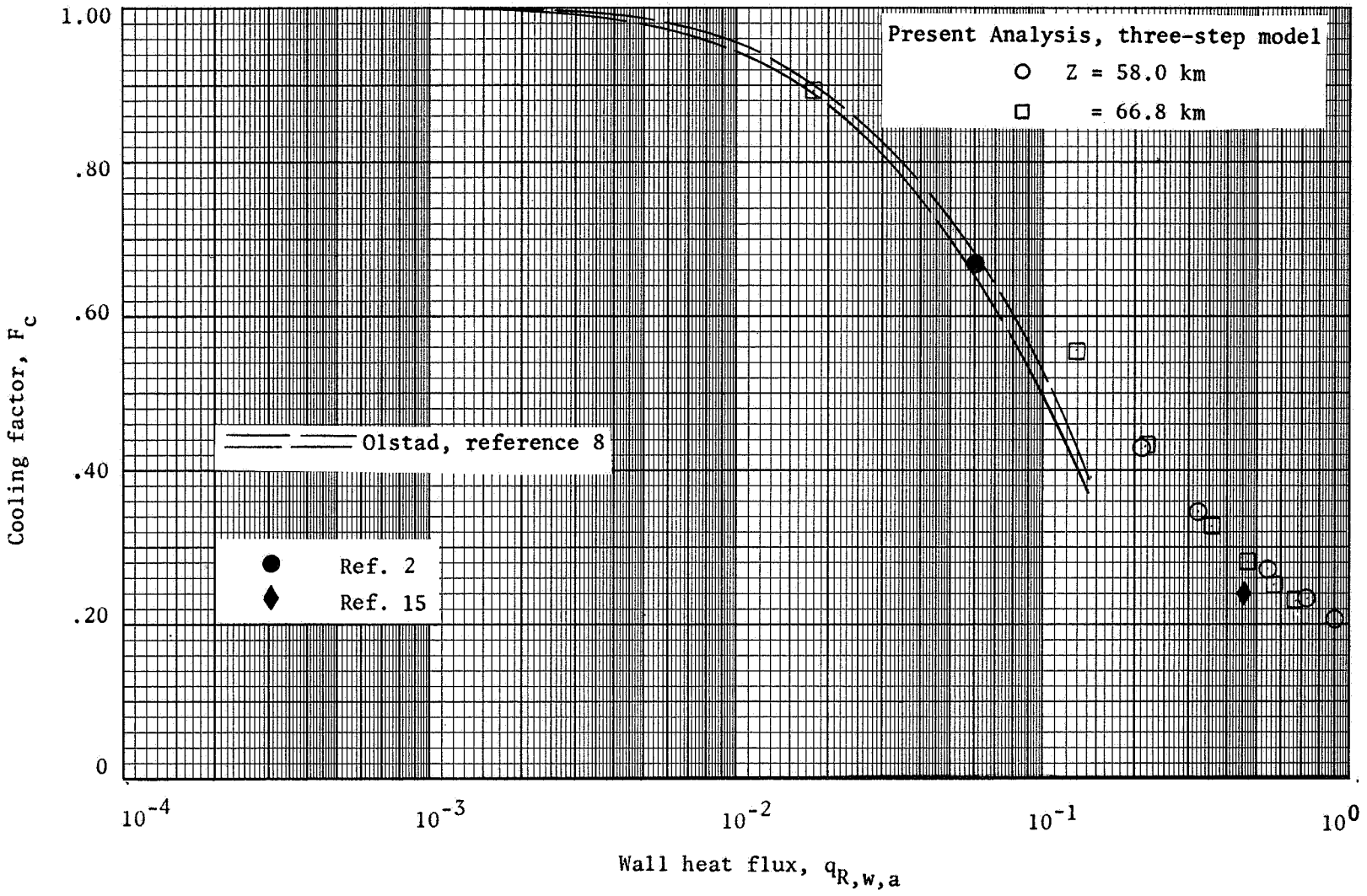

(c) $\bar{V}_\infty$ = 15 240 m/s.

Figure 13.- Continued.

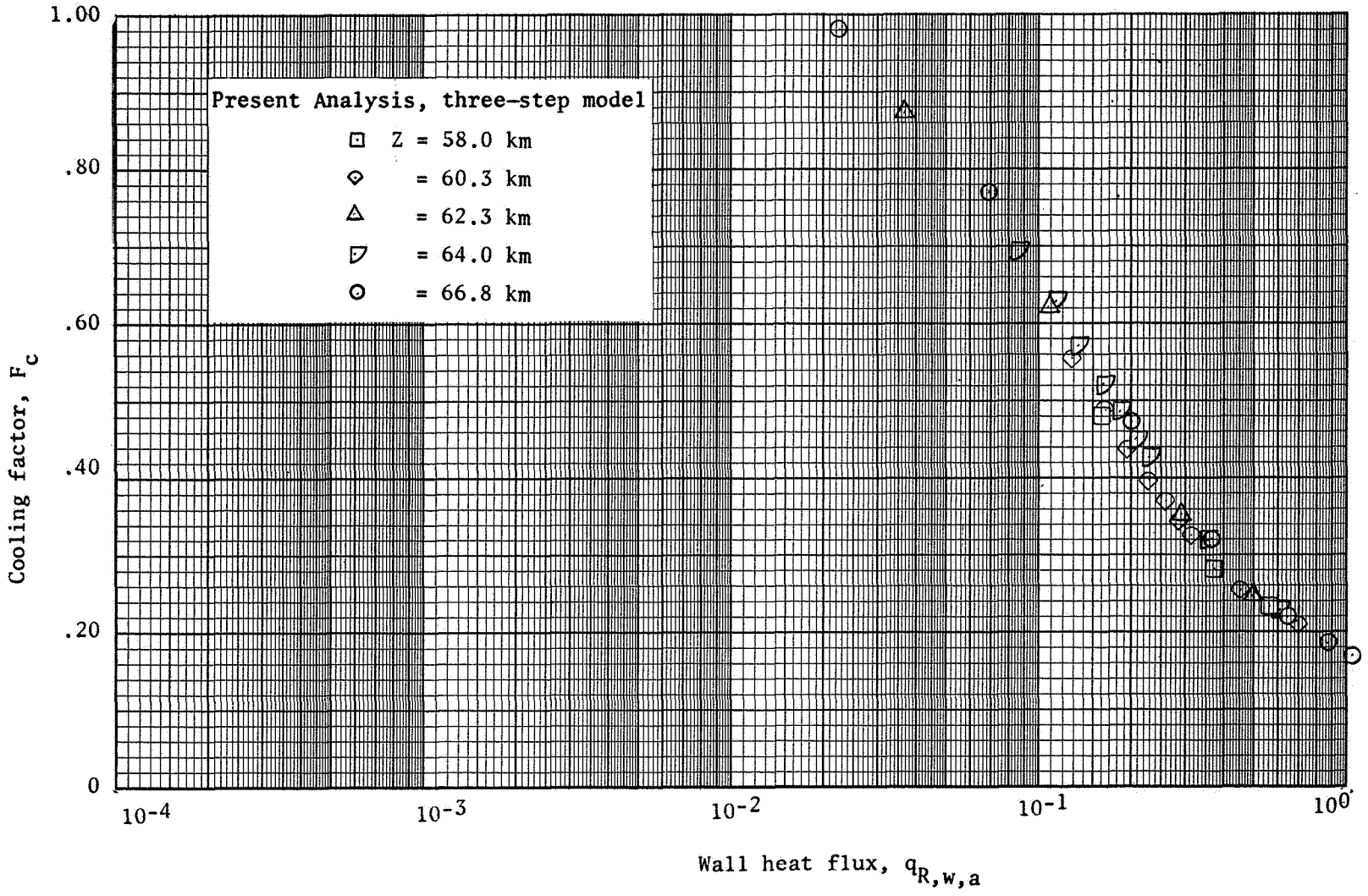

(d) $\overline{V}_\infty$ = 18 280 m/s.

Figure 13.- Concluded.

NATIONAL AERONAUTICS AND SPACE ADMINISTRATION
WASHINGTON, D. C. 20546

OFFICIAL BUSINESS

FIRST CLASS MAIL

POSTAGE AND FEES PAID
NATIONAL AERONAUTICS AND
SPACE ADMINISTRATION

POSTMASTER: If Undeliverable (Section 158 Postal Manual) Do Not Return

"The aeronautical and space activities of the United States shall be conducted so as to contribute . . . to the expansion of human knowledge of phenomena in the atmosphere and space. The Administration shall provide for the widest practicable and appropriate dissemination of information concerning its activities and the results thereof."

—NATIONAL AERONAUTICS AND SPACE ACT OF 1958

NASA SCIENTIFIC AND TECHNICAL PUBLICATIONS

TECHNICAL REPORTS: Scientific and technical information considered important, complete, and a lasting contribution to existing knowledge.

TECHNICAL NOTES: Information less broad in scope but nevertheless of importance as a contribution to existing knowledge.

TECHNICAL MEMORANDUMS: Information receiving limited distribution because of preliminary data, security classification, or other reasons.

CONTRACTOR REPORTS: Scientific and technical information generated under a NASA contract or grant and considered an important contribution to existing knowledge.

TECHNICAL TRANSLATIONS: Information published in a foreign language considered to merit NASA distribution in English.

SPECIAL PUBLICATIONS: Information derived from or of value to NASA activities. Publications include conference proceedings, monographs, data compilations, handbooks, sourcebooks, and special bibliographies.

TECHNOLOGY UTILIZATION PUBLICATIONS: Information on technology used by NASA that may be of particular interest in commercial and other non-aerospace applications. Publications include Tech Briefs, Technology Utilization Reports and Notes, and Technology Surveys.

Details on the availability of these publications may be obtained from:

SCIENTIFIC AND TECHNICAL INFORMATION DIVISION

NATIONAL AERONAUTICS AND SPACE ADMINISTRATION

Washington, D.C. 20546